Entanglement in quantum field theory via wavelet representations

Daniel J. George,[1,2,3,*] Yuval R. Sanders,[1,3,4] Mohsen Bagherimehrab,[5,6,7] Barry C. Sanders,[5] and Gavin K. Brennen[1,3]

[1]*Department of Physics and Astronomy, Macquarie University, Sydney, NSW 2109, Australia*
[2]*Sydney Quantum Academy, Sydney, NSW 2000, Australia*
[3]*ARC Centre of Excellence in Engineered Quantum Systems, Macquarie University, Sydney, NSW 2109, Australia*
[4]*Centre for Quantum Software and Information, University of Technology Sydney, Sydney, NSW 2007, Australia*
[5]*Institute for Quantum Science and Technology, University of Calgary, Calgary, Alberta T2N 1N4, Canada*
[6]*Chemical Physics Theory Group, Department of Chemistry, University of Toronto, Toronto, Ontario M5G 1Z8, Canada*
[7]*Department of Computer Science, University of Toronto, Toronto, Ontario M5S 2E4, Canada*

(Received 11 May 2022; accepted 29 July 2022; published 26 August 2022)

Quantum field theory (QFT) describes nature using continuous fields, but physical properties of QFT are usually revealed in terms of measurements of observables at a finite resolution. We describe a multiscale representation of free scalar bosonic and Ising model fermionic QFTs using wavelets. Making use of the orthogonality and self-similarity of the wavelet basis functions, we demonstrate some well-known relations such as scale-dependent subsystem entanglement entropy and renormalization of correlations in the ground state. We also find some new applications of the wavelet transform as a compressed representation of ground states of QFTs which can be used to illustrate quantum phase transitions via fidelity overlap and holographic entanglement of purification.

DOI: 10.1103/PhysRevD.106.036025

I. INTRODUCTION

Quantum information has provided new perspectives into quantum field theories (QFT), such as using entanglement as a way to characterize quantum phases [1], and quantum algorithms for simulating scattering cross sections in QFTs that are exponentially faster than classical algorithms [2]. Other insights include the study of coarse-graining and renormalization from a quantum information perspective [3], and the harvesting of entanglement from vacuum states of QFTs [4,5]. Recently, it was shown that quantum field theories can be represented in a way that organizes properties at multiple scales using a wavelet functional basis, referred to as a multiscale representation [6,7]. Wavelet-based multiscale representations of QFT have proved particularly well suited for studying the holographic principle [8–11] and renormalization physics [12,13].

Several recent works have demonstrated a connection between wavelets and tensor-network- or quantum-circuit-based representations of quantum states. For example, Evenbly and White [12] used a Daubechies wavelet basis to analytically construct the tensors in a multiscale entanglement renormalization ansatz (MERA) description of a ground state of massless (critical) fermions on a 1D lattice. Haegeman *et al.* [14] showed how to rigorously construct quantum circuits that approximate metallic states of massless fermions on 1D and 2D lattices based on a discrete wavelet transform using an approximate Hilbert pair. For quadratic bosonic systems on a lattice, Witteveen and Walter [15] developed a scale-invariant entanglement renormalization procedure based on biorthogonal wavelets that disentangles the wavelet output at each step. Finally, Witteveen *et al.* [16] found a procedure for constructing MERA-based quantum circuits that rigorously approximate the continuum correlation functions for the massless Dirac conformal field theory.

In this paper we derive the wavelet-based multiscale representations of two types of QFT: the one-dimensional Ising fermionic QFT and free scalar bosonic QFT, both introduced in Sec. II. Wavelet-based multiscale representations can be understood as a more nuanced form of discretization, in which the continuum Hamiltonian is expressed as an infinite number of terms corresponding to ever-finer length scales. A minimum length scale is then enforced by the truncation of terms at finer length scales. We demonstrate that a number of established results remain

*Corresponding author. dan.george@hdr.mq.edu.au

valid when using these representations, and suggest some advantages of such representations for identifying phase transitions. We present a brief introduction to the relevant aspects of the wavelet formalism in Sec. III.

The main results of our paper are contained in Sec. IV. We show that wavelet-based multiscale representations provide natural access to entanglement renormalization physics. In Sec. IV A we show numerically that the two-point correlators of a coarse-grained QFT decay algebraically in a scale-invariant manner at the critical point and with an exponential decay with correlation length given by the inverse renormalized mass in the massive phase. In Sec. IV B we reproduce using a wavelet-based discretization the results of Calabrese and Cardy [1] for subsystem entanglement in noninteracting bosonic and fermionic QFTs. Calabrese and Cardy [1] model the QFT with a lattice spin system that is treated as a discrete approximation to the true continuum theory, justifiable by computing a continuum limit (see, e.g., Sec. II in [17]). We demonstrate that the discretization of these field theories using wavelet scale modes reproduces the correct scaling of entanglement in both gapped and gapless phases of the theories and we connect the phenomenological cutoff length to the scale of our scale modes.

In Sec. IV D we consider a multiscale wavelet representation of the ground state for a fermionic Ising QFT, and show that selection of a subsystem consisting of a small number of coarse-grained modes amounts to a form of lossy compression, capturing the physics of the global pure state up to some error. We demonstrate the utility of this approach for approximating the fidelity overlap between ground states adjacent in some parameter, and therefore as a witness for quantum phase transitions, where the direct calculation or measurement of fidelity over the global state may be computationally or experimentally infeasible. In Sec. IV E we show that the entanglement of purification for a reduced quantum state, the calculation of which quickly becomes unwieldy for large numbers of modes, can be well approximated by a coarse-grained state. This is significant in the context of the work by Umemoto and Takayanagi [18], in which the authors conjecture that the entanglement of purification in conformal field theories (CFTs) is equal to the minimal-area cross section of the entanglement wedge. Finally, in Secs. V and VI we summarize our results and conclude with an outlook for further applications of our methodology.

II. BACKGROUND

We focus here on noninteracting one-dimensional fermionic and bosonic quantum field theories, due to their mathematical simplicity and frequent use as a starting point for perturbative models, especially in quantum algorithms [2,7]. They are exactly solvable and therefore allow for direct comparison of wavelet-based results to known continuum physics.

A. Ising fermionic continuum QFT

The Hamiltonian density for the free Ising model fermionic quantum field theory in one dimension is (see Eq. (11a) in [17])

$$\hat{\mathcal{H}}_{\mathrm{f}}(x,t) \coloneqq \frac{1}{2}(-\mathrm{i}\hat{\boldsymbol{b}}^T(x,t)\boldsymbol{Z}\partial_x\hat{\boldsymbol{b}}(x,t) + m_0\hat{\boldsymbol{b}}^T(x,t)\boldsymbol{Y}\hat{\boldsymbol{b}}(x,t)), \tag{1}$$

where $\hat{\boldsymbol{b}}(x,t) \equiv \left[\begin{smallmatrix}\hat{b}_0(x,t)\\ \hat{b}_1(x,t)\end{smallmatrix}\right]$ is the spinor of Majorana mode operators at location x, m_0 is the bare mass, and $\boldsymbol{Z} = \left[\begin{smallmatrix}1 & 0\\ 0 & -1\end{smallmatrix}\right]$ and $\boldsymbol{Y} = \left[\begin{smallmatrix}0 & -\mathrm{i}\\ \mathrm{i} & 0\end{smallmatrix}\right]$ are the usual Pauli matrices. Note that the spinor components satisfy the equal-time Majorana anticommutation relation

$$\{\hat{b}_\sigma(x), \hat{b}_{\sigma'}(x')\} = 2\delta_{\sigma,\sigma'}\delta(x-x') \tag{2}$$

for $\sigma, \sigma' \in \{0,1\}$. The Majorana mode operators have units of inverse square root of length. In the massless phase, the theory is described by the Ising model CFT with central charge $c = 1/2$.

B. Free scalar bosonic continuum QFT

The Hamiltonian density for the free scalar bosonic quantum field theory in d spatial dimensions is (see Eq. (11) in [7])

$$\hat{\mathcal{H}}_{\mathrm{b}}(\boldsymbol{x},t) = \frac{1}{2}(\hat{\Pi}^2(\boldsymbol{x},t) + (\nabla\hat{\Phi}(\boldsymbol{x},t))^2 + m_0^2\hat{\Phi}^2(\boldsymbol{x},t)), \tag{3}$$

where the field operator $\hat{\Phi}(\boldsymbol{x},t)$ and its conjugate momentum $\hat{\Pi}(\boldsymbol{x},t) \coloneqq \partial_t\hat{\Phi}(\boldsymbol{x},t)$ satisfy the canonical equal-time commutation relations

$$[\hat{\Phi}(\boldsymbol{x},t), \hat{\Pi}(\boldsymbol{x}',t)] = \mathrm{i}\delta^{(d)}(\boldsymbol{x}-\boldsymbol{x}')\mathbb{1}, \text{ and} \tag{4}$$

$$[\hat{\Phi}(\boldsymbol{x},t), \hat{\Phi}(\boldsymbol{x}',t)] = [\hat{\Pi}(\boldsymbol{x},t), \hat{\Pi}(\boldsymbol{x}',t)] = 0. \tag{5}$$

Most of the results below are for the $d = 1$ case where the field operator is dimensionless. In the massless phase, the theory is described by the free bosonic CFT with central charge $c = 1$.

C. Entanglement entropy scaling

An important physical characterization of QFT is given by subsystem entanglement of ground states. The entanglement entropy of a bipartite pure state $|\psi\rangle_{AB}$ is given by the von Neumann entropy: $S_A = -\mathrm{Tr}(\rho_A \log \rho_A)$, where the subsystem state with support on region A is $\rho_A = \mathrm{Tr}_B[|\psi\rangle_{AB}\langle\psi|_{AB}]$. For most of the work here, the QFT is assumed to be in one spatial dimension over the compact interval $[0, X)$ with specified boundary conditions. A subsystem A consists of a single subinterval $[0, X_A)$ of the compact interval $[0, X)$. The relevant results are given in Calabrese and Cardy [1] and Holzhey *et al.* [19]:

$$S_A^{\text{critical,periodic}}(x) = \frac{c}{3}\log\left(\frac{\sin(\pi x)}{\pi\varepsilon}\right) + \text{constant}, \quad (6)$$

$$S_A^{\text{critical,open}}(x) = \frac{c}{6}\log\left(\frac{\sin(\pi x)}{\pi\varepsilon}\right) + \text{constant}, \quad (7)$$

$$S_A^{\text{noncritical}}(x) = (\text{ boundary points}) \times \frac{c}{6}\log(m_0\varepsilon), \quad (8)$$

which correspond to entropy scaling in the massless (critical) case, for periodic (see Eq. (1) in [1]) and open boundary conditions (see Eq. (2) in [1]), and in the massive (noncritical) case (see Eq. (1) in [1]). Here ε is the ultraviolet cutoff length, c the central charge of the relevant CFT, and m_0 the mass. Note also that (8) is valid only for the subsystem length $X_A \gg 1/m_0$.

III. WAVELET-BASED DISCRETIZATION OF QUANTUM FIELD THEORY

A. Definition

Here we use the Daubechies family of wavelets, a family indexed by a positive integer $\mathcal{K}$ (with $\mathcal{K} = 1$ corresponding to the well-known Haar wavelet), which has additional beneficial properties such as compactness, allowing study of spatially separated operators and zero-valued moments. The Daubechies family of compactly supported wavelets can be defined as follows. For an alternative introduction, see Sec. II in [20], or for a more thorough treatment, see Chap. 7 in [21] or Chap. 5 in [22].

The wavelet basis is defined in terms of a pair of functions, the scale and wavelet functions, here denoted by s and w respectively. Elsewhere these are sometimes referred to as the father and mother wavelets and denoted ϕ and ψ, respectively.

A function $s \in \mathcal{L}^2(\mathbb{R})$ is called a scale function if it satisfies the orthonormality condition

$$\forall\, \ell \in \mathbb{Z}\colon \int_{\mathbb{R}} s(x)s(x-\ell)\mathrm{d}x = \delta_{0,\ell} \quad (9)$$

and if, for any other function $f \in \mathcal{L}^2(\mathbb{R})$,

$$f(x) \overset{\text{a.e.}}{=} \lim_{r\to\infty} \sum_{\ell\in\mathbb{Z}} \sqrt{2^r}\, c_\ell^{(r)} s(2^r x - \ell), \text{ with} \quad (10)$$

$$c_\ell^{(r)} \coloneqq \sqrt{2^r} \int_{\mathbb{R}} f(x)s(2^r x - \ell)\mathrm{d}x, \quad (11)$$

where the symbol $\overset{\text{a.e.}}{=}$ means "equal almost everywhere," which is to say that $f(x)$ is equal to the right-hand side for all x except for a measure-zero set. For notational convenience, we denote the scale function at scale (or resolution) r and position ℓ by

$$\forall\, r, \ell \in \mathbb{Z}\colon s_\ell(x) \coloneqq s(x-\ell), \quad s_\ell^{(r)}(x) \coloneqq \sqrt{2^r} s_\ell(2^r x). \quad (12)$$

The scale and wavelet functions at scale r are defined recursively as a linear combination of scale functions at scale $r+1$, with weights given by the set of scale filter coefficients $\{h_\ell\}$, $\ell \in \mathbb{Z}$:

$$s_\ell^{(r)}(x) = \sum_{\ell'\in\mathbb{Z}} h_{\ell'} s_{\ell+\ell'}^{(r+1)}(x), \quad (13)$$

$$w_\ell^{(r)}(x) \coloneqq \sum_{\ell'\in\mathbb{Z}} (-1)^{\ell'} h_{\Lambda-\ell'-1} s_{\ell+\ell'}^{(r+1)}(x) \quad (14)$$

where Λ is the number of nonzero filter coefficients such that $h_\ell = 0$ if $\ell < 0$ or $\ell \geq \Lambda$, and a similar notational convention has been adopted for the wavelet functions as in (12). Specification of these coefficients uniquely determines the wavelet basis.

For the Daubechies-$\mathcal{K}$ (db$\mathcal{K}$) wavelet, the scale filter coefficients $\{h_\ell\}$ are uniquely determined for $\mathcal{K} = 1$, and up to reflection for any integer $\mathcal{K} > 1$, by requiring simultaneously that the first $\mathcal{K}$ moments vanish:

$$\int \mathrm{d}x\, w_0^{(r)}(x)x^p = 0, \quad p = 0, 1, \ldots, \mathcal{K}-1, \quad (15)$$

and that the number of nonzero coefficients, Λ, is minimized. It turns out that this occurs for $\Lambda = 2\mathcal{K}$ filter coefficients. Additionally, it can be shown that the scale and wavelet functions at scale 0 are supported on the interval $[0, 2\mathcal{K}-1]$, and that the first differentiable scale function is the scale function of the db3 wavelet (see page 239 in [22]), hence its predominant use in this paper.

In addition to Eq. (9), the scale and wavelet functions further obey the orthonormality properties

$$\forall\, \ell, \ell', r, r' \in \mathbb{Z} \text{ s.t. } r' \geq r\colon \int_{\mathbb{R}} s_\ell^{(r)}(x) w_{\ell'}^{(r')}(x)\mathrm{d}x = 0, \quad (16)$$

$$\forall\, \ell, \ell', r, r' \in \mathbb{Z}\colon \int_{\mathbb{R}} w_\ell^{(r)}(x) w_{\ell'}^{(r')}(x)\mathrm{d}x = \delta_{\ell,\ell'}\delta_{r,r'}. \quad (17)$$

The fixed-resolution subspace $\mathcal{S}_r$ at resolution $r \in \mathbb{Z}$, along with the associated wavelet subspace $\mathcal{W}_r$, can be defined in terms of scale and wavelet functions at resolution r:

$$\mathcal{S}_r \coloneqq \text{span}\{s_\ell^{(r)} | \ell \in \mathbb{Z}\}, \quad \mathcal{W}_r \coloneqq \text{span}\{w_\ell^{(r)} | \ell \in \mathbb{Z}\} \quad (18)$$

where $\mathcal{S}_r, \mathcal{W}_r \subset \mathcal{L}^2(\mathbb{R})$. Equation (14) implies that $\mathcal{S}_r, \mathcal{W}_r \subset \mathcal{S}_{r+1}$, and from this and the orthogonality conditions in Eq. (17), it follows that the space $\mathcal{W}_r$ is precisely the orthogonal complement of $\mathcal{S}_r$ in $\mathcal{S}_{r+1}$, and therefore

$$\mathcal{S}_r = \mathcal{S}_{r-1} \oplus \mathcal{W}_{r-1}. \tag{19}$$

The wavelet transform in one dimension at scale r is defined as the isomorphism

$$\boldsymbol{W}^{(r)}\colon \mathcal{S}_r \to \mathcal{S}_{r-1} \oplus \mathcal{W}_{r-1} \tag{20}$$

which functions as the basis transform

$$\{s_\ell^{(r)}\} \to \{s_\ell^{(r-1)}\} \cup \{w_\ell^{(r-1)}\}, \quad \ell \in \mathbb{Z}. \tag{21}$$

The d-level wavelet transform for $d > 1$ is defined by the recursive application of $\boldsymbol{W}^{(r)}$ resulting in

$$\boldsymbol{W}_d^{(r)}\colon \mathcal{S}_r \to \mathcal{S}_{r-d} \oplus \mathcal{W}_{r-d} \oplus \cdots \oplus \mathcal{W}_{r-1} \tag{22}$$

which functions as the basis transform

$$\{s_\ell^{(r)}\} \to \{s_\ell^{(r-d)}\} \cup \{w_\ell^{(r-d)}\} \cup \{w_\ell^{(r-d+1)}\} \cup \cdots \cup \{w_\ell^{(r-1)}\}, \quad \ell \in \mathbb{Z}. \tag{23}$$

In this paper we identify $r = 0$ with the coarsest scale modes and consider scales $0 \le r < n$, and therefore make use of the n-level wavelet transform acting at scale n:

$$\boldsymbol{W}_n^{(n)}\colon \mathcal{S}_n \to \mathcal{S}_0 \oplus \mathcal{W}_0 \oplus \cdots \oplus \mathcal{W}_{n-1}. \tag{24}$$

The numeric construction of the single-level and multilevel discrete wavelet transform from wavelet coefficients is discussed in detail in Bagherimehrab *et al.* (see Appendix A in [23]).

B. Fixed-resolution and multiresolution representations

It is useful to define a fixed-scale representation in terms of the action of an idempotent projection operator. Define for each scale r the projection operator mapping from the vector space $\mathcal{L}^2(\mathbb{R})$ to the subspace $\mathcal{S}_r$ defined in Eq. (18):

$$\mathrm{proj}_r\colon \mathcal{L}^2(\mathbb{R}) \to \mathcal{S}_r\colon f \mapsto \sum_{\ell\in\mathbb{Z}} \langle s_\ell^{(r)}|f\rangle s_\ell^{(r)} = \sum_{\ell\in\mathbb{Z}} c_\ell^{(r)} s_\ell^{(r)} \tag{25}$$

where $|s_\ell^{(r)}\rangle$ are the scale functions in Eq. (14) with $\ell \in \mathbb{Z}$ and the inner product corresponds to the coefficients $c_\ell^{(r)}$ defined in Eq. (11). This projection operator is discussed in more depth by Daubechies [22].

Both fermionic and bosonic Hamiltonians include the action of a derivative operator, the projection of which requires some care since the derivative is not strictly in $\mathcal{L}^2(\mathbb{R})$. Specifically, the α-order derivative $\frac{\mathrm{d}^\alpha}{\mathrm{d}x^\alpha}$ acts only upon a proper vector (but not Hilbert) subspace of $\mathcal{L}^2(\mathbb{R})$ corresponding to the set of functions whose derivatives up to α order also belong to $\mathcal{L}^2(\mathbb{R})$. The projected derivative operator is

$$\left.\frac{\mathrm{d}^\alpha}{\mathrm{d}x^\alpha}\right|_r \coloneqq \mathrm{proj}_r \circ \frac{\mathrm{d}^\alpha}{\mathrm{d}x^\alpha} \circ \mathrm{proj}_r, \tag{26}$$

subject to the requirement that f is a square-integrable function with α continuous and square-integrable derivatives. Wavelet analysis of these Hamiltonians is therefore restricted to scale functions with the requisite properties. The α-order derivative of an arbitrary α-order differentiable function f is then

$$\left.\frac{\mathrm{d}^\alpha f}{\mathrm{d}x^\alpha}\right|_r = \sum_{\ell,\ell'} \left\langle s_\ell^{(r)}\middle|f\right\rangle \left\langle s_{\ell'}^{(r)}\middle|\frac{\mathrm{d}^\alpha}{\mathrm{d}x^\alpha}\middle|s_\ell^{(r)}\right\rangle s_{\ell'}^{(r)} \tag{27}$$

and the action of $\frac{\mathrm{d}^\alpha}{\mathrm{d}x^\alpha}|_r$ is entirely determined by the coefficients

$$\left\langle s_{\ell'}^{(r)}\middle|\frac{\mathrm{d}^\alpha}{\mathrm{d}x^\alpha}\middle|s_\ell^{(r)}\right\rangle = \int \mathrm{d}x\, s_{\ell'}^{(r)}(x) \frac{\mathrm{d}^\alpha}{\mathrm{d}x^\alpha} s_\ell^{(r)}(x) \tag{28}$$

$$= 2^{\alpha r} \int \mathrm{d}x\, s_{\ell'-\ell}(x) \frac{\mathrm{d}^\alpha}{\mathrm{d}x^\alpha} s(x) \tag{29}$$

$$=: 2^{\alpha r} \Delta_{\ell'-\ell}^{(\alpha)} \tag{30}$$

henceforth referred to as the derivative overlap coefficients.

Beylkin [20] showed how to compute the derivative overlap coefficients for any scale functions specified by filter coefficients $h_\ell, \ell \in \{0, \ldots, 2\mathcal{K}-1\}$ (all other coefficients are set to zero) by first defining the autocorrelation coefficients (see Eq. (3.19) in [20])

$$a_\ell \coloneqq 2\sum_{\ell'} h_\ell h_{\ell'}. \tag{31}$$

Subject to a condition on the number of vanishing moments of the resulting wavelet function, Beylkin proved (see Eqs. (4.3)–(4.4) in [20]) that the derivative overlap coefficients $\Delta_\ell^{(\alpha)}$ constitute the unique solution to the system of equations

$$\Delta_\ell^{(\alpha)} = 2^\alpha \Delta_{2\ell}^{(\alpha)} + \frac{1}{2}\sum_{k=1}^{\mathcal{K}} a_{2k-1}(\Delta_{2\ell-2k+1}^{(\alpha)} + \Delta_{2\ell+2k-1}^{(\alpha)}); \tag{32}$$

$$\sum_{\ell=-2\mathcal{K}+2}^{2\mathcal{K}-2} \ell^\alpha \Delta_\ell^{(\alpha)} = (-1)^\alpha \alpha! \tag{33}$$

and for a Daubechies wavelet it can be shown that (see Eqs. (3.51)–(3.52) in [20])

$$a_{2n-1} = \frac{(-1)^{n-1}}{(\mathcal{K}-n)!(\mathcal{K}+n-1)!(2n-1)} \times \left(\frac{(2\mathcal{K}-1)!}{4^{\mathcal{K}-1}(\mathcal{K}-1)!}\right)^2. \tag{34}$$

Note that these autocorrelation coefficients are rational, from which it follows that the derivative overlap coefficients $\Delta_\ell^{(\alpha)}$ are also rational.

C. One-dimensional Ising fermionic QFT

A wavelet-based multiscale representation of a continuum Hamiltonian over a length interval $[0, X)$ consists of a (countably) infinite sum of terms. Initial terms correspond to the scale modes at the coarsest length scale (scale $r = 0$, length of order $2^{-r} = 1$), and progress to wavelet modes at finer and finer length scales (down to scale $r = \infty$). A minimum scale n (length of order 2^{-n}) is applied by truncating terms corresponding to scales $r > n$, and is equivalent to projecting the Hamiltonian onto the scale subspace $\mathcal{S}_n$. The number of modes V in the system is then

$$V \coloneqq 2^n X. \tag{35}$$

Equivalently, the Hamiltonian of a system can be directly expressed in terms of V scale modes at scale n and the multiscale representation from scales 0 to n is then recovered via the application of the n-level wavelet transform. This latter process is superficially similar to discretization, and it is often easier to use the language of discretization (e.g., "wavelet-discretized modes"); however, it should be remembered that the underlying concepts are distinct.

The scale Majorana modes spanning the scale subspace $\mathcal{S}_r$ are defined in terms of the continuum modes like so:

$$\hat{\boldsymbol{b}}_\ell^{(r;\mathrm{s})} \coloneqq \begin{bmatrix} \hat{b}_{\ell,0}^{(r;\mathrm{s})} \\ \hat{b}_{\ell,1}^{(r;\mathrm{s})} \end{bmatrix}, \qquad \hat{b}_{\ell,\sigma}^{(r;\mathrm{s})} \coloneqq \int_0^X \mathrm{d}x\, s_\ell^{(r)}(x)\hat{b}_\sigma(x). \tag{36}$$

In the fermionic case we consider antiperiodic boundary conditions, which correspond to the even parity sector. The discretized Majorana modes $\hat{b}_{\ell,\sigma}^{(r;s)}$ satisfy anticommutation relations analogous to those of Eq. (2) but with the Dirac delta replaced with a Kronecker delta. Also note that our restriction to a finite-sized subspace of $\mathcal{L}^2(\mathbb{R})$ ensures that only finitely many of these discretized Majorana operators are nonzero.

The wavelet Majorana modes are defined analogously by

$$\hat{b}_{\ell,\sigma}^{(r;\mathrm{w})} \coloneqq \int_0^X \mathrm{d}x\, w_\ell^{(r)}(x)\hat{b}_\sigma(x), \tag{37}$$

and complement the scale-discretized Majorana modes $\hat{b}_{\ell,\sigma}^{(r;\mathrm{s})}$.

To project the Hamiltonian from Eq. (1) to the subspace $\mathcal{S}_n$ defined in Eq. (18) corresponding to the coarse-graining scale n, conjugate $\hat{\mathcal{H}}_\mathrm{f}$ with the canonical projection operator $\mathrm{proj}(n)$ from Eq. (25). This results in the discrete Hamiltonian

$$\hat{H}_\mathrm{f}^{(n)} = -\frac{\mathrm{i}}{2}\sum_{\ell,\ell'\in\mathbb{Z}} 2^n \Delta_{\ell'}^{(1)} \hat{\boldsymbol{b}}_\ell^{(n;s)\intercal} \boldsymbol{Z} \hat{\boldsymbol{b}}_{\ell+\ell'}^{(n;s)} + \frac{1}{2} m_0 \sum_{\ell\in\mathbb{Z}} \hat{\boldsymbol{b}}_\ell^{(n;s)\intercal} \boldsymbol{Y} \hat{\boldsymbol{b}}_\ell^{(n;s)}, \tag{38}$$

where the symbol $\Delta_\ell^{(\alpha)}$ refers to the ℓth derivative overlap coefficient of order α as defined in Eq. (30), and m_0 is the bare (unrenormalized) mass at scale n and should be chosen accordingly.

The quadratic structure of the Hamiltonian can be made explicit by reexpressing $\hat{H}_\mathrm{f}^{(n)}$ as

$$\hat{H}_\mathrm{f}^{(n)} = -\frac{\mathrm{i}}{2}\sum_{\substack{\ell,\ell'\in\mathbb{Z}\\ \sigma,\sigma'\in\{0,1\}}} Q_{\ell,\sigma;\ell',\sigma'}^{(n)} \hat{b}_{\ell,\sigma}^{(n;s)} \hat{b}_{\ell',\sigma'}^{(n;s)}, \tag{39}$$

$$Q_{\ell,\sigma;\ell',\sigma'}^{(n)} \coloneqq (-1)^\sigma 2^n \Delta_{\ell'-\ell}^{(1)} \delta_{\sigma,\sigma'} + m_0 \delta_{\ell,\ell'}(\sigma' - \sigma). \tag{40}$$

Note that $Q_{\ell',\sigma';\ell,\sigma}^{(n)} = -Q_{\ell,\sigma;\ell',\sigma'}^{(n)}$ because $\Delta_{-\ell}^{(1)} = -\Delta_\ell^{(1)}$.

The coefficients $Q_{\ell,\sigma;\ell',\sigma'}^{(n)}$ are effectively the entries of a $2V \times 2V$ matrix $\boldsymbol{Q}^{(n)}$ acting on a vector space with basis vectors indexed by (ℓ, σ). The matrix $\boldsymbol{Q}^{(n)}$ is real and antisymmetric and hence has pure imaginary eigenvalues $\pm\mathrm{i}\omega_k^{(n)}$, $k \in \{\frac{1}{2}, \frac{3}{2}, \ldots, V - \frac{1}{2}\}$ where $\omega_k^{(n)} \in \mathbb{R}$. To find these eigenvalues, observe that due to the applied antiperiodic boundary conditions, the submatrix consisting of entries $Q_{\ell,0;\ell',0}^{(n)}$ is the antiperiodic analog of a circulant matrix, with a negative sign applied to the entries below the main diagonal. Hence it can be diagonalized using a half-integer-indexed discrete Fourier transform, resulting in submatrix eigenvalues

$$\lambda_k = \sum_{\ell=0}^{V-1} 2^n \Delta_\ell^{(1)} \mathrm{e}^{2\mathrm{i}\pi k\ell/V} = \mathrm{i}\sum_{\ell=1}^{2\mathcal{K}-2} 2^{n+1} \Delta_\ell^{(1)} \sin\left(\frac{2\pi k\ell}{V}\right) \tag{41}$$

for $k \in \{\frac{1}{2}, \frac{3}{2}, \ldots, V - \frac{1}{2}\}$, where the second equality is obtained by using the antisymmetry and periodicity of the derivative overlap coefficients $\Delta_\ell^{(1)}$ and noting that $\Delta_0^{(1)} = 0$. Similarly the eigenvalues of the submatrix $Q_{\ell,1;\ell',1}$ are $-\lambda_k$. Therefore $\boldsymbol{Q}^{(k)}$ is unitarily equivalent to the direct sum of V 2×2 matrices:

$$\boldsymbol{Q}^{(n)} \sim \bigoplus_{k=\frac{1}{2}}^{V-\frac{1}{2}} \begin{bmatrix} \lambda_k & -m_0 \\ m_0 & -\lambda_k \end{bmatrix}. \tag{42}$$

The eigenvalues of each 2×2 matrix are then $\pm\mathrm{i}\omega_k \coloneqq \pm\sqrt{-m_0^2 + \lambda_k^2}$ and so

$$\omega_k^{(n)} = \sqrt{m_0^2 + \left(\sum_{\ell=1}^{2\mathcal{K}-2} 2^{n+1}\Delta_\ell^{(1)} \sin\left(\frac{2\pi k\ell}{V}\right)\right)^2}. \quad (43)$$

In the continuum limit as $n \to \infty$,

$$\omega_k^{(n)} \to \sqrt{m_0^2 + \left(\frac{4\pi k}{X}\sum_\ell \ell\Delta_\ell^{(1)}\right)^2} = \sqrt{m_0^2 + \left(\frac{2\pi k}{X}\right)^2}, \quad (44)$$

where the first simplification uses the small-angle approximation for sine and the second the antisymmetry of the derivative overlap coefficients $\Delta_\ell^{(1)}$ together with Eq. (33). This recovers the well-known dispersion relation for the continuum Ising model.

The projected Hamiltonian in Eq. (39) is quadratic in the fermionic operators. Therefore, its ground state is a Gaussian state. Any Gaussian state is fully characterized by its covariance matrix. For a fermionic system, this matrix is obtained from a two-point correlation of the system's fermionic operators [24].

The entries of the covariance matrix $\mathbf{\Gamma}^{(n)}$ for the ground state of the projected Hamiltonian are defined so that

$$\Gamma^{(n)}_{\ell,\sigma;\ell',\sigma'} := \mathrm{i}\langle[\hat{b}^{(n;s)}_{\ell,\sigma}, \hat{b}^{(n;s)}_{\ell',\sigma'}]\rangle \quad (45)$$

where $\langle\cdot\rangle := \mathrm{Tr}(\cdot\rho)$. $\mathbf{\Gamma}^{(n)}$ can be calculated by first observing that entries of the covariance matrix $\bar{\mathbf{\Gamma}}$ for the uncoupled Majorana operators $\hat{\bar{\boldsymbol{b}}}$ are

$$\bar{\Gamma}_{\ell,\sigma;\ell',\sigma'} = \mathrm{i}\langle[\hat{\bar{b}}_{\ell,\sigma}, \hat{\bar{b}}_{\ell',\sigma'}]\rangle = \delta_{\ell,\ell'}(\sigma - \sigma'), \quad (46)$$

which follows from the definition of the ground state and from the anticommutation relations for Majorana fermions.

Let $\boldsymbol{O}^{(n)}$ be the orthogonal transformation matrix that uncouples Majorana operators at scale n: $\hat{\bar{\boldsymbol{b}}} := \boldsymbol{O}^{(n)}\hat{\boldsymbol{b}}^{(n;s)}$. Then

$$\mathbf{\Gamma}^{(n)} = \boldsymbol{O}^{(n)\intercal}\bar{\mathbf{\Gamma}}\boldsymbol{O}^{(n)}. \quad (47)$$

Calculation of $\boldsymbol{O}$ is via symplectic diagonalization[1] of the coupling matrix $\boldsymbol{Q}^{(n)}$ which takes the analogous form

$$\boldsymbol{Q}^{(n)} = \boldsymbol{O}^{(n)\intercal}\begin{bmatrix} 0 & \mathbf{\Omega} \\ -\mathbf{\Omega} & 0 \end{bmatrix}\boldsymbol{O}^{(n)}, \quad (48)$$

where $\mathbf{\Omega}$ is the diagonal matrix with diagonal entries ω_k.

Our next step is to approximate the fine-scale correlator $\langle\hat{b}^{(n;s)}_{\ell,\sigma}\hat{b}^{(n;s)}_{\ell',\sigma'}\rangle$. As this is an expectation value of anticommuting operators, its value is zero whenever $\sigma = \sigma'$. Translational symmetry requires that $\langle\hat{b}^{(n;s)}_{\ell,0}\hat{b}^{(n;s)}_{\ell',1}\rangle = \langle\hat{b}^{(n;s)}_{0,0}\hat{b}^{(n;s)}_{\ell'-\ell,1}\rangle$, and together with anticommutation it further follows that $\langle\hat{b}^{(n;s)}_{0,0}\hat{b}^{(n;s)}_{-\ell,1}\rangle = -\langle\hat{b}^{(n;s)}_{0,0}\hat{b}^{(n;s)}_{\ell,1}\rangle$. We derive expressions for the correlators in the Appendix.

D. One-dimensional bosonic QFT

To obtain a multiscale representation of the bosonic continuum field theory, we again first define the projection of the bosonic field and conjugate momentum operators onto the scale subspace $\mathcal{S}_r$. Let

$$\hat{\Phi}^{(r)}_\ell(t) := \int_0^X \mathrm{d}x\, s^{(r)}_\ell(x)\hat{\Phi}(x,t) \quad (49)$$

and

$$\hat{\Pi}^{(r)}_\ell(t) := \int_0^X \mathrm{d}x\, s^{(r)}_\ell(x)\hat{\Pi}(x,t) \quad (50)$$

be the canonical position and momentum field operators projected onto the scale subspace $\mathcal{S}_r$. The scale field and conjugate momentum operators satisfy commutation relations analogous to those of Eq. (4) but with the Dirac delta replaced with the Kronecker delta. The wavelet field and conjugate momentum operators are defined analogously to Eqs. (36) and (37).

Projecting the bosonic Hamiltonian $\hat{\mathcal{H}}_\mathrm{b}(x,t)$ from Eq. (3) to a scale subspace $\mathcal{S}_n$ with the projection operator from Eq. (25) results in

$$\hat{H}^{(n)}_\mathrm{b} := \frac{1}{2}\sum_{\ell\in\mathbb{Z}}\hat{\Pi}^{(n;\mathrm{s})}_\ell\hat{\Pi}^{(n;\mathrm{s})}_\ell + \frac{1}{2}\sum_{\ell,\ell'\in\mathbb{Z}}\hat{\Phi}^{(n;\mathrm{s})}_\ell K^{(n)}_{\ell\ell'}\hat{\Phi}^{(n;\mathrm{s})}_{\ell'}, \quad (51)$$

where, for notational simplicity, dependence on time has been dropped, and

$$K^{(n)}_{\ell,\ell'} := m_0^2\delta_{\ell,\ell'} - 4^n(\Delta^{(2)}_{\ell'-\ell} + \Delta^{(2)}_{\ell'-(\ell+N)}) \quad (52)$$

corresponding to periodic boundary conditions. The spectrum of the projected periodic Hamiltonian is then

$$\omega_k^{(n)} = \sqrt{m_0^2 - \sum_{\ell=-2\mathcal{K}+2}^{2\mathcal{K}-2} 4^n\Delta_\ell^{(2)}\cos\left(\frac{2\pi k\ell}{V}\right)}. \quad (53)$$

In the continuum limit as $n \to \infty$,

[1]In the case that the eigenvalues of $\boldsymbol{Q}^{(n)}$ are all nonzero, numeric construction of $\boldsymbol{O}^{(n)}$ is simple: of the eigenvectors of $\boldsymbol{Q}^{(n)}$ having eigenvalues $\pm\mathrm{i}\omega_k$, let $\{\boldsymbol{w}_k\}$ be all the eigenvectors corresponding to eigenvalues of either $+\mathrm{i}\omega_k$ or $-\mathrm{i}\omega_k$. The rows of $\boldsymbol{O}^{(n)}$ are then the normalized real and imaginary components of $\boldsymbol{w}_k$, that is, $\mathrm{Re}\,\boldsymbol{w}_k/\|\mathrm{Re}\,\boldsymbol{w}_k\|$ followed by $\mathrm{Im}\,\boldsymbol{w}_k/\|\mathrm{Im}\,\boldsymbol{w}_k\|$.

$$\omega_k^{(n)} \to \sqrt{m_0^2 - \sum_\ell 4^n \Delta_\ell^{(2)} \left(1 - \frac{1}{2}\left(\frac{2\pi k \ell}{V}\right)^2\right)} \tag{54}$$

$$= \sqrt{m_0^2 + \left(\frac{2\pi k}{X}\right)^2} \tag{55}$$

using the cosine small-angle approximation, Eq. (33) and $\sum_\ell \Delta_\ell^{(2)} = 0$ (see Eq. (3.35) in [20]). In the thermodynamic limit $X \to \infty$, $2\pi k/X$ becomes a continuum parameter that is the momentum of the continuum theory, recovering the well-known dispersion relation for the continuum bosonic field theory.

The covariance matrix for a bosonic state is defined as [24,25]

$$\Gamma_{\ell,\ell'}^{(n)} := \langle \{\hat{r}_\ell^{(n;\mathrm{s})}, \hat{r}_{\ell'}^{(n;\mathrm{s})}\}\rangle, \tag{56}$$

where $\hat{\boldsymbol{r}}^{(n;\mathrm{s})} := (\hat{\Phi}_0^{(n;\mathrm{s})}, \ldots, \hat{\Phi}_{N-1}^{(n;\mathrm{s})}, \hat{\Pi}_0^{(n;\mathrm{s})}, \ldots, \hat{\Pi}_{N-1}^{(n;\mathrm{s})})$ is the vector of canonical scale operators at scale n. For the ground state of the Hamiltonian in Eq. (51), the covariance matrix is simply $\boldsymbol{\Gamma}^{(n)} = \boldsymbol{\Gamma}_\Phi^{(n)} \oplus \boldsymbol{\Gamma}_\Pi^{(n)}$ where $\boldsymbol{\Gamma}_\Pi^{(n)} := \sqrt{\boldsymbol{K}^{(n)}}$ and $\boldsymbol{\Gamma}_\Phi^{(n)} := (\boldsymbol{\Gamma}_\Pi^{(n)})^{-1}$ [24].

IV. RESULTS

A. Renormalization in multiscale correlators

As described in Eq. (24), the Hilbert space spanned by scale modes at scale n is equivalent to the Hilbert space spanned by coarser scale modes at scale 0 completed by wavelet modes from scales $0 \le r < n$. This allows us to express correlations between wavelet modes at some scales $r < n$ in terms of a linear combination of finer scale modes at scale n. This constitutes the so-called bulk/boundary correspondence where the wavelet modes (and coarse scale modes) comprise the bulk with two dimensions indexed by position and scale, while the finer scale modes comprise the one-dimensional boundary with one position index. The general expression for the correlators of wavelet mode operators $\hat{A}^{(\mathrm{w})}$ and $\hat{B}^{(\mathrm{w})}$ at scales r and r' and positions ℓ and ℓ' in terms of equivalent scale mode operators at scale $n \gg r$ is [11]

$$\begin{aligned}\langle \hat{A}_\ell^{(r;\mathrm{w})} \hat{B}_{\ell'}^{(r';\mathrm{w})}\rangle = 2^{-n} 2^{(r+r')/2} \sum_{j=2^{n-r}\ell}^{2^{n-r}(\ell+2\mathcal{K}-1)} \sum_{j'=2^{n-r'}\ell'}^{2^{n-r'}(\ell'+2\mathcal{K}-1)} \\ \times w_0^{(0)}(2^{r-n}(j - 2^{n-r}\ell + 1)) \\ \times w_0^{(0)}(2^{r'-n}(j' - 2^{n-r'}\ell' + 1)) \langle \hat{A}_j^{(n;\mathrm{s})} \hat{B}_{j'}^{(n;\mathrm{s})}\rangle.\end{aligned} \tag{57}$$

1. Fermionic case

For a theory with bare mass m_0 defined at the scale n, the fine-scale correlators are (see the Appendix for derivation)

$$\langle \hat{b}_{0,0}^{(n;s)} \hat{b}_{\ell,1}^{(n;s)}\rangle = \frac{\mathrm{i}}{V} \sum_{k \in S} \mathrm{e}^{-2\mathrm{i}\theta_k} \mathrm{e}^{-\mathrm{i}2\pi\ell k/V}, \tag{58}$$

$$\text{where } \theta_k = \arctan \frac{-q_k}{m_0 + \sqrt{m_0^2 + q_k^2}}, \tag{59}$$

$$\text{and } q_k = 2 \sum_{j=1}^{2\mathcal{K}-2} \Delta_j^{(1)} \sin \frac{2\pi j k}{V}. \tag{60}$$

In the massless case this simplifies to

$$\langle \hat{b}_{0,0}^{(n;s)} \hat{b}_{\ell,1}^{(n;s)}\rangle = \begin{cases} \frac{-2}{V \sin(\pi\ell/V)} & \ell \text{ odd}, \\ 0 & \ell \text{ even}. \end{cases} \tag{61}$$

As per Singh and Brennen [11] the correlator between wavelet modes at different scales $r, r' < n$ is

$$\langle \hat{b}_{0,0}^{(r;\mathrm{w})} \hat{b}_{\ell,1}^{(r';\mathrm{w})}\rangle \approx \sum_{j,j'=0}^{V-1} \langle \hat{b}_{0,0}^{(n;s)} \hat{b}_{j-j',1}^{(n;s)}\rangle f_{j,0}^{n,r} f_{j',\ell}^{n,r'}, \tag{62}$$

$$f_{j,\ell}^{n,r} = \int dx\, s_j^{(n)}(x) w_\ell^{(r)}(x), \tag{63}$$

with other expressions given by translational symmetry and anticommutation. Correlations at the same scale $r = r'$ can be approximated in the continuum limit for r sufficiently far from the boundary. Assuming $r \ll n$, let $2^{r-n}\ell \to x$, treating x as a continuous variable so that $\delta\ell = 2^{n-r}dx$, and replacing sums by integrals $\sum_{m=0}^{2^{n-r}(2\mathcal{K}-1)} \to 2^{n-r} \int_0^{2\mathcal{K}-1} dx$, results in

$$\begin{aligned}\langle \hat{b}_{0,0}^{(r;\mathrm{w})} \hat{b}_{\ell,1}^{(r;\mathrm{w})}\rangle = \mathrm{i}2^{-r} \int_0^{2\mathcal{K}-1} dx \int_\ell^{2\mathcal{K}-1+\ell} dx'\, w_0^{(0)}(x) \\ \times w_0^{(0)}(x' - \ell) \langle \hat{b}_0(x) \hat{b}_1(x')\rangle.\end{aligned} \tag{64}$$

In the massless phase, for large n, the continuous correlator can be replaced by the discrete correlator from Eq. (61). Assuming $r \gg 0$ leads to $\sin(\pi 2^{-r}(x - x')/V) \approx \pi 2^{-r}(x - x')/V$. Restrict attention to correlations longer range than the size of the wavelet modes, i.e., $\ell > 2\mathcal{K} - 1$, so that the integrals satisfy $\int_0^{2\mathcal{K}-1} dx w_0^0(x) w_0^0(x - \ell) = 0$. Define the new variable $x'' = x' - \ell$, then

$$\langle \hat{b}^{(r;\mathrm{w})}_{0,0} \hat{b}^{(r;\mathrm{w})}_{\ell,1} \rangle = \mathrm{i} \int dx \int dx'' \frac{w^{(0)}_0(x) w^{(0)}_0(x'')}{\pi((x-x'')-\ell)}$$
$$= -\frac{\mathrm{i}}{\pi\ell} \int dx \int dx'' \, w^{(0)}_0(x) w^{(0)}_0(x'') \sum_{k=0}^{\infty} \frac{(x-x'')^k}{\ell^k}$$
$$= -\frac{\mathrm{i}}{\pi} \sum_{k=0}^{\infty} \frac{1}{\ell^{k+1}} \sum_{t=0}^{k} \binom{k}{t} (-1)^t \langle x^t \rangle_w \langle x^{k-t} \rangle_w. \tag{65}$$

Here $\langle f(x) \rangle_w \equiv \int f(x) w^0_0(x) dx$ and for general functions must be computed numerically. However the wavelet moments $\langle x^a \rangle_w = \int x^a w^0_0(x) dx$ can be computed recursively in closed form (see e.g., [6]). The dominant term in the correlation is determined by the lowest nontrivial wavelet moment:

$$\langle \hat{b}^{(k;\mathrm{w})}_{0,0} \hat{b}^{(k;\mathrm{w})}_{\ell,1} \rangle \approx \frac{\mathrm{i}(-1)^{\mathcal{K}}}{\pi \ell^{2\mathcal{K}+1}} \times \binom{2\mathcal{K}}{\mathcal{K}} \langle x^{\mathcal{K}} \rangle^2_w. \tag{66}$$

Figure 1 (top) shows this expression plotted with direct calculation of the multiscale correlators by application of the wavelet transform to the covariance matrix.

For the massive phase, analytic expressions for the correlators are more difficult to obtain; however, the numerical results, plotted in Fig. 1 (bottom), demonstrate exponential falloff with separation with an inverse correlation length given by renormalized mass

$$\tilde{m} = 2^{n-r} m_0. \tag{67}$$

2. Bosonic case

Singh and Brennen [11] (Eqs. B5 and B8 there) show that in the massless phase, the same-scale field-field and momenta-momenta correlations for separations $\ell \gg 2\mathcal{K}-1$ and $r \ll n$ are

$$\langle \hat{\Phi}^{(r;\mathrm{w})}_0 \hat{\Phi}^{(r;\mathrm{w})}_\ell \rangle \approx -\frac{2^{n-r}}{4\pi \ell^{2\mathcal{K}} \mathcal{K}} \times \binom{2\mathcal{K}}{\mathcal{K}} \langle x^{\mathcal{K}} \rangle^2_w, \tag{68}$$

$$\langle \hat{\Pi}^{(r;\mathrm{w})}_0 \hat{\Pi}^{(r;\mathrm{w})}_\ell \rangle \approx \frac{2^{r-n}(2\mathcal{K}+1)}{2\pi \ell^{2\mathcal{K}+2}} \times \binom{2\mathcal{K}}{\mathcal{K}} \langle x^{\mathcal{K}} \rangle^2_w. \tag{69}$$

Figure 2 shows these approximations plotted against direct calculation of the multiscale correlators from the covariance matrix.

In the massive phase, the bulk correlations are exponentially decaying in all directions. For $\tilde{m} \gg 1$ and separations $\ell \gg 2\mathcal{K}-1$, the coarse-grained ($r \ll n$) field-field and momenta-momenta correlations are (see Eqs. B15 and B16 in [11])

$$\langle \hat{\Phi}^{(r;\mathrm{w})}_0 \hat{\Phi}^{(r;\mathrm{w})}_\ell \rangle \approx -\frac{2^{n-r} e^{-\ell \tilde{m}}}{\sqrt{8\pi \ell \tilde{m}}} \langle e^{-\tilde{m}x} \rangle_w \langle e^{\tilde{m}x} \rangle_w, \tag{70}$$

$$\langle \hat{\Pi}^{(r;\mathrm{w})}_0 \hat{\Pi}^{(r;\mathrm{w})}_\ell \rangle \approx 2^{r-n} e^{-\ell \tilde{m}} \sqrt{\frac{\tilde{m}}{8\pi \ell^3}} \langle e^{-\tilde{m}x} \rangle_w \langle e^{\tilde{m}x} \rangle_w. \tag{71}$$

Figure 3 shows these expressions plotted with numerical calculations of the multiscale covariance matrix.

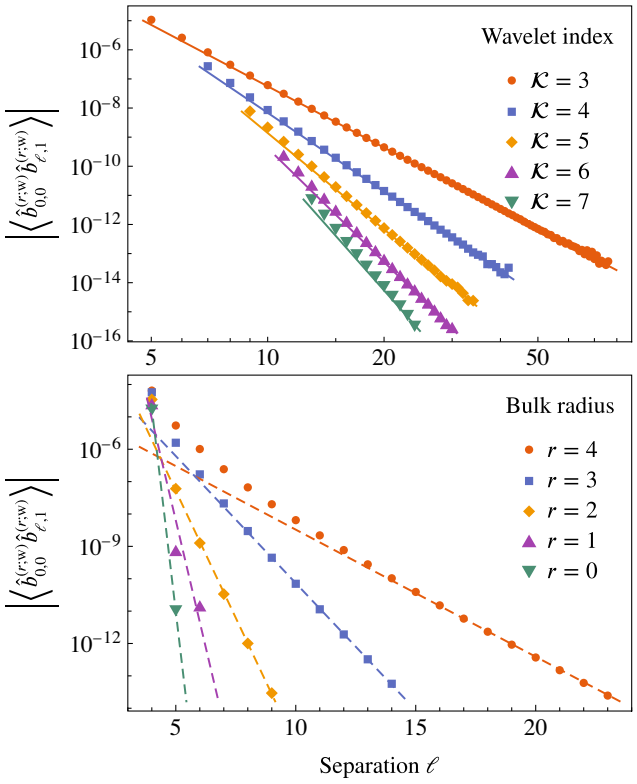

FIG. 1. Bulk same-scale wavelet-wavelet correlations $|\langle \hat{b}^{(r;\mathrm{w})}_{0,0} \hat{b}^{(r;\mathrm{w})}_{\ell,1} \rangle|$ at scale $r < n$ as a function of spatial separation ℓ for $X = 16$, $n = 6$, $V = 2^n X = 1024$. Top: the critical fermionic Ising model field theory $\hat{H}^{(n)}_{\mathrm{f}}$, correlations at radius $r = 4$ plotted for various Daubechies wavelet indices $\mathcal{K}$. Solid lines are plots of Eq. (66). Bottom: the massive fermionic field theory with $m_0 = 0.2$, correlations at various radii for $\mathcal{K} = 3$. Dotted lines are a joint linear regression assuming $2^{(n-r)}$ dependence. The correlations fall off exponentially as $\mathrm{e}^{-1.13\ell\tilde{m}}$, indicating scale-dependent mass renormalization, Eq. (67).

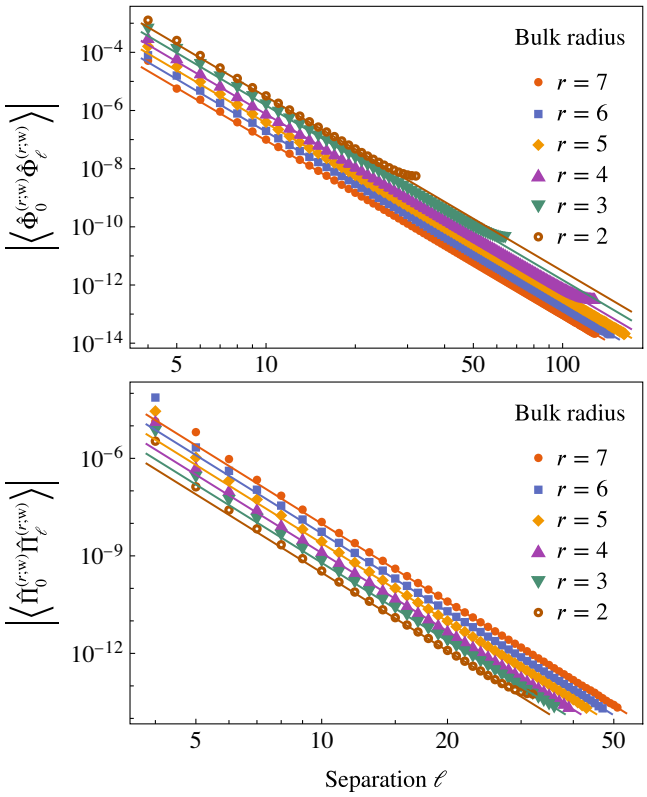

FIG. 2. Bulk same-scale wavelet-wavelet correlations for the massless bosonic field theory $\hat{H}_{\mathrm{b}}^{(n)}$ at scale $r < n$ as a function of spatial separation ℓ for $X = 16$, $n = 8$, $V = 2^n X = 4096$ modes with periodic boundary conditions. Daubechies $\mathcal{K} = 3$ wavelets were used. Top: field-field correlations $|\langle \hat{\Phi}_0^{(r;\mathrm{w})} \hat{\Phi}_\ell^{(r;\mathrm{w})} \rangle|$ with lines from Eq. (68). Bottom: momenta-momenta correlations $|\langle \hat{\Pi}_0^{(r;\mathrm{w})} \hat{\Pi}_\ell^{(r;\mathrm{w})} \rangle|$ with lines from Eq. (69).

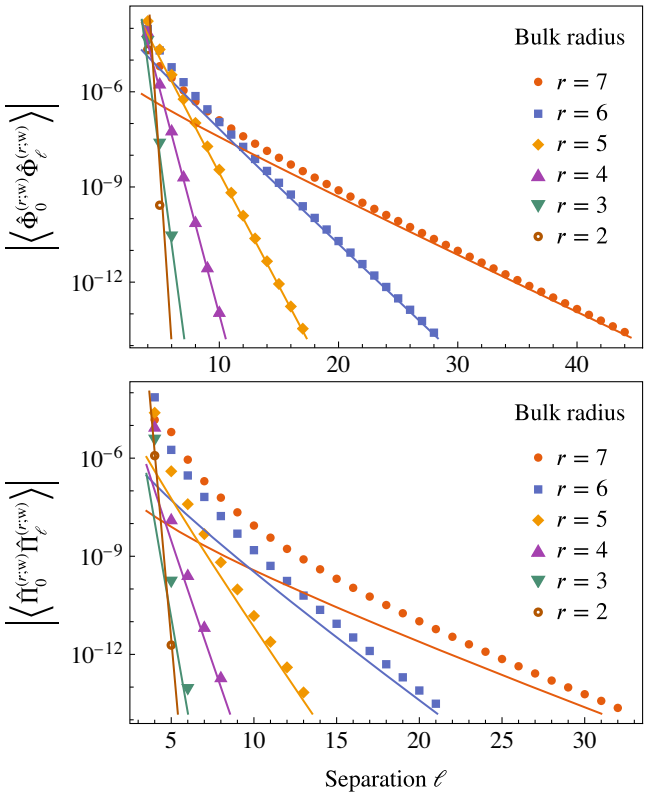

FIG. 3. Bulk same-scale wavelet-wavelet correlations for the massive bosonic field theory $\hat{H}_b^{(n)}$ at scale $r < n$ as a function of spatial separation ℓ for $X = 16$, $n = 8$, $V = 2^n X = 4096$ modes with periodic boundary conditions. Mass is $m_0 = 0.2$ and Daubechies $\mathcal{K} = 3$ wavelets were used. Top: field-field correlations $|\langle \hat{\Phi}_0^{(r;\mathrm{w})} \hat{\Phi}_\ell^{(r;\mathrm{w})} \rangle|$ with lines from Eq. (70). Bottom: momenta-momenta correlations $|\langle \hat{\Pi}_0^{(r;\mathrm{w})} \hat{\Pi}_\ell^{(r;\mathrm{w})} \rangle|$ with lines from Eq. (71).

B. Entanglement entropy of subsystems in 1D

1. Subsystem specification

In the wavelet scale basis, as in the canonical basis, the covariance matrix $\mathbf{\Gamma}^A$ of a subsystem A is obtained by selecting a subset of the rows and columns of the system's covariance matrix $\mathbf{\Gamma}$. Suppose that the subsystem A of a system containing V scale modes at scale n over the interval $[0, X)$ is an interval of the form $[x_{\min}, x_{\max}) := [\ell_{\min}/2^n, \ell_{\max}/2^n)$ for integers $0 \le \ell_{\min} < \ell_{\max} \le V$. The subset of modes $s_\ell^{(n)}$ retained belong to the interval $[x_{\min}, x_{\max})$ and correspond to $\ell \in \{\ell_{\min}, \ldots, \ell_{\max} - 1\}$. Setting $V_A := \ell_{\max} - \ell_{\min}$, the resulting covariance matrix $\mathbf{\Gamma}^A$ is of size $V_A \times V_A$. The total length of the interval $[x_{\min}, x_{\max})$, or length of the subsystem A, is $X_A = V_A/2^n$.

In these calculations a subsystem A with $V_A \le V/2$ modes is selected to be an interval of the form $[0, X_A)$. The subsystem's modes are taken to be less than $V/2$ as the entropy of two subsystems with $V/2 - V_A$ and $V/2 + V_A$ modes are the same. Figure 4 shows the entropy plots for the massless bosonic and fermionic theories with different boundary conditions.

2. Fermionic case

The covariance matrix $\mathbf{\Gamma}$ for a fermionic state is real and antisymmetric, and satisfies $\mathbf{\Gamma}^2 \ge -\mathbb{1}$ ([26], p. 2). Therefore its eigenvalues are all purely imaginary and come in positive and negative pairs; i.e., the set of eigenvalues is $\{\pm \mathrm{i}\sigma_\ell\}$. Moreover, $|\sigma_\ell| \le 1$. Note that $\{\pm\sigma_\ell\}$ is the set of singular values of $\mathbf{\Gamma}$ which is equal to the set of eigenvalues of $\mathrm{i}\mathbf{\Gamma}$. The entanglement entropy of an N-mode fermionic Gaussian state ρ^A can then be expressed in terms of the singular values $\{\sigma_\ell^A\}$ of its covariance matrix $\mathbf{\Gamma}^A$ as (see [26], page 2)

$$S(\rho^A) = \sum_{\sigma_\ell^A \in [0,1]} H\left(\frac{1 + \sigma_\ell^A}{2}\right), \tag{72}$$

where $H(x) := -x \log_2(x) - (1 - x) \log_2(1 - x)$ is the binary entropy function.

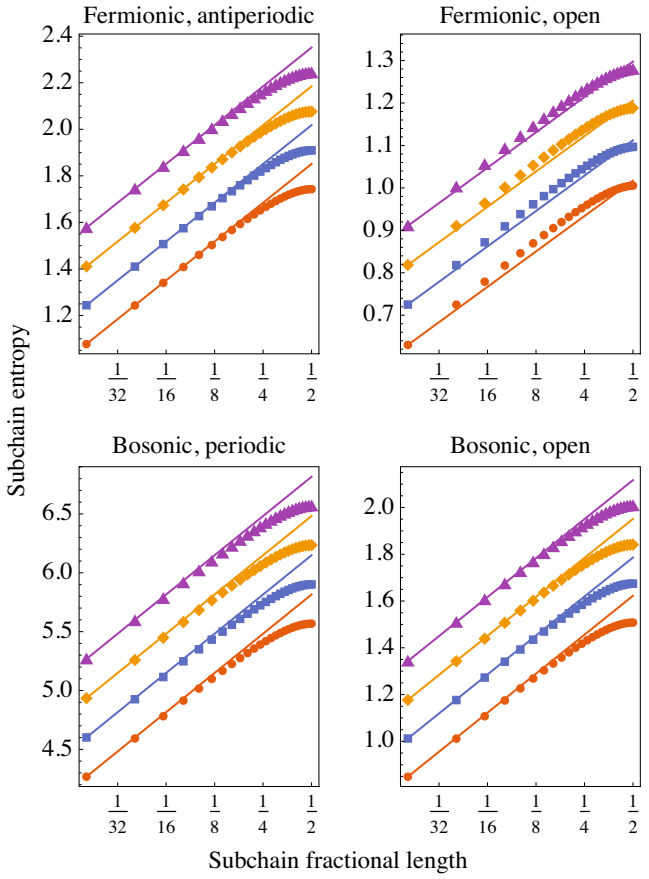

FIG. 4. Plots of the critical subsystem entropy for the fermionic and bosonic theories with (anti)periodic and open boundaries. Each of the data points correspond to a subinterval of the indicated fractional length. A boundary point of the subinterval always coincides with a boundary point of the whole interval. Each curve depicts the system at a different resolution with number of modes $V = 500$ (orange circles, bottom), $V = 1000$ (blue squares), $V = 2000$ (yellow diamonds), or $V = 4000$ (purple triangles, top). Entropy increases with resolution. In the (anti)periodic case, we encounter a singularity in the zero-mass limit and therefore set $m_0 = 10^{-8}$ for the fermionic system and $m_0 = 10^{-4}$ for the bosonic system. The solid lines are used to indicate the central charge, and have slope $1/6$ in the antiperiodic fermionic case, $1/12$ in the open fermionic case, $1/3$ in the periodic bosonic case, and $1/6$ for the open bosonic cases. These slopes correspond to the expected central charges of $c = 1/2$ for the Ising model CFT and $c = 1$ for the free bosonic CFT in the context of Eqs. (6) and (7). The leftmost point of each line is chosen to match the leftmost data point.

For the massive fermionic theory, we observe that the entanglement entropy of a subsystem is constant as a function of the subsystem's length in different scales, and this constant increases with the scale r. This is expected from the entanglement area law. For the massless theory, we observe that the functional form of the Calabrese-Cardy relations are correct as given in Sec. II C, and the central charge is correct by means of a line with slope equal to $c/3$ and $c/6$, for periodic and open boundary conditions respectively. Figure 4 shows the entropy plots for the massless theory with different boundary conditions.

3. Bosonic case

The covariance matrix $\mathbf{\Gamma}$ for a bosonic state is a real and positive-definite symmetric matrix, and satisfies $\mathbf{\Gamma} + i\mathbf{\Omega}/2 \geq 0$ ([25], page 2) where

$$\mathbf{\Omega} := \begin{pmatrix} \mathbf{0} & \mathbb{1}_N \\ -\mathbb{1}_N & \mathbf{0} \end{pmatrix}. \tag{73}$$

Williamson's theorem states that any symmetric and positive-definite matrix, such as the covariance matrix $\mathbf{\Gamma}$, can be decomposed as $\mathbf{\Gamma} = \boldsymbol{S}^T(\mathbf{\Lambda} \oplus \mathbf{\Lambda})\boldsymbol{S}$ ([25], p. 18), where $\boldsymbol{S}$ is a symplectic matrix and $\mathbf{\Lambda}$ is a diagonal matrix whose spectrum $\{\lambda_\ell\}$ is equal to the set of positive eigenvalues of $i\mathbf{\Omega}\mathbf{\Gamma}$ ([24], page 28). The eigenvalues of $\mathbf{\Lambda}$ are called the symplectic eigenvalues of the covariance matrix $\mathbf{\Gamma}$. $\mathbf{\Gamma} + i\mathbf{\Omega}/2 \geq 0$ further implies that $\lambda_\ell \geq 1/2$.

The entanglement entropy of an N-mode bosonic Gaussian state ρ^A can then be expressed in terms of the symplectic eigenvalues of its covariance matrix $\mathbf{\Gamma}^A$ as [27]

$$S(\rho^A) = \sum_{\ell=1}^{2N} f(\lambda_\ell^A), \tag{74}$$

where

$$f(\lambda) := \left(\lambda + \frac{1}{2}\right)\log_2\left(\lambda + \frac{1}{2}\right) - \left(\lambda - \frac{1}{2}\right)\log_2\left(\lambda - \frac{1}{2}\right). \tag{75}$$

Similar to the fermionic case, we again observe that the functional form of the Calabrese-Cardy relations are correct as given in Sec. II C.

4. Cutoff scaling behavior

For a massless bosonic field theory in one spatial dimension with periodic boundary conditions the subsystem entanglement is related to the ultraviolet cutoff parameter ε as per Eq. (6) with $c = 1$. We computed the half-chain entropy in a wavelet basis ($\mathcal{K} = 3$) for resolutions $V = 2^n X$ with $X = 32$ and for $n = 0, \ldots, 7$ (mass was technically $m_0 = 10^{-4}$ to avoid a singularity in the zero-mass limit). The numerical results demonstrate linear scaling in n with a least-squares fit of $S = 6.23 + 0.333n$, in agreement with the expected scaling law $\varepsilon \propto \frac{1}{V} = \frac{1}{2^n X}$.

C. Entanglement entropy in 2D

Since there is no direct analog for the fermionic Ising model in two dimensions, we consider only bosonic systems here. The scaling of subsystem entanglement

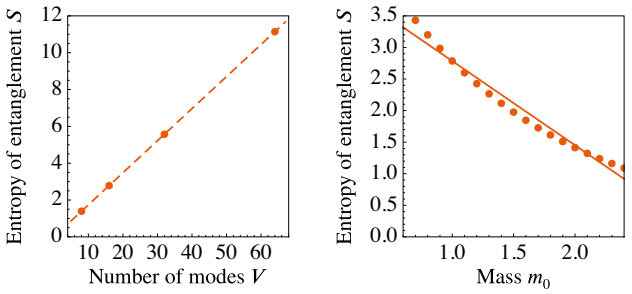

FIG. 5. Entropy of entanglement for a $V \times \frac{V}{2}$-mode subsystem of a $V \times V$ two-dimensional system as a function of the number of modes $V = 2^n X$, with $X = 8$. The one-dimensional area of the boundary is V. Left: entropy of entanglement against number of modes for $n \in \{0, 1, 2, 3\}$, with mass $m_0 = 1$, demonstrating expected linear scaling of S with V (dashed line is the least-squares fit corresponding to $\varepsilon = 3.88$). Right: same as left but as a function of mass with $n = 1$. The solid line is Eq. (76), with a slope of $-A_\perp/12 = -4/3$ and the intercept is $A_\perp/\varepsilon = 4.12$ using ε from the fit on the left (note the values coincide at $m_0 = 1$ as expected). While the slope is reasonably accurate over this mass range, it is apparent higher order terms contribute.

entropy depends on the number of spatial dimensions. For two spatial dimensions, to first order in $A_\perp$, the scaling for a free bosonic QFT is [28]

$$S \approx \frac{A_\perp}{\varepsilon} - \frac{1}{12} A_\perp m_0, \tag{76}$$

where $A_\perp$ is the area of the one-dimensional subsystem boundary and ε is the ultraviolet cutoff of the field theory. The scaling behavior of the massive bosonic field theory in two dimensions in a wavelet basis is demonstrated in Fig. 5.

D. Discriminating quantum phases via fidelity overlap

One witness of a quantum phase transition (QPT) is a sudden drop in the overlap fidelity between ground states of Hamiltonians straddling a critical point [29]. Specifically, for a Hamiltonian which experiences a QPT as a function of one parameter g, the witness is

$$F = |\langle \Psi(g_+)|\Psi(g_-)\rangle|, \tag{77}$$

where $g_\pm = g \pm \delta/2$, and $|\Psi(g)\rangle$ is the ground state of the Hamiltonian with parameter g. Here δ is some increment small enough to resolve the change in F.

As in the Appendix, the ground state of the fermionic Ising model, where the relevant parameter is $g = m_0$, is specified by the condition

$$\hat{\eta}_k |\Psi\rangle = 0, \tag{78}$$

where the normal fermionic modes are defined in terms of the momenta annihilation and creation operators $\hat{p}_k, \hat{p}_k^\dagger$ as

$$\hat{\eta}_k = \cos\theta_k \hat{p}_k + \mathrm{i} \sin\theta_k \hat{p}_{-k}^\dagger, \tag{79}$$

$$\theta_k = \cos^{-1}\left[\frac{-(m_0 + \omega_k)}{\sqrt{(m_0 + \omega_k)^2 + q_k^2}}\right], \tag{80}$$

$$q_k = 2 \sum_{\ell=1}^{2K-2} \Delta_\ell^{(1)} \sin\left(\frac{2\pi k \ell}{V}\right). \tag{81}$$

Negative momenta modes are defined by positive indexing via $-k \equiv V - k$. For antiperiodic boundary conditions the set of allowable positive momenta k is $k \in S_L = \{\frac{1}{2}, \frac{3}{2}, \ldots, \frac{V-1}{2}\}$. Using the inverse Jordan-Wigner transformation and ordering qubits in pairs $\{(k, -k)\}_{k \in S_L}$ results in expressions $\hat{p}_k = [\prod_{j<k} \boldsymbol{Z}_j \boldsymbol{Z}_{-j}]\sigma_k^+$ and $\hat{p}_{-k}^\dagger = [\prod_{j<k} \boldsymbol{Z}_j \boldsymbol{Z}_{-j}]\boldsymbol{Z}_k \sigma_{-k}^-$, where $\sigma_k^\pm \equiv \frac{1}{2}(\boldsymbol{X}_k \pm \mathrm{i}\boldsymbol{Y}_k)$ are the usual raising and lowering operators acting on mode k. The ground state can then be written as a tensor product of entangled qubit pairs

$$|\Psi\rangle = \bigotimes_{k \in S_L} (\cos\theta_k |1\rangle_k |1\rangle_{-k} + \mathrm{i} \sin\theta_k |0\rangle_k |0\rangle_{-k}). \tag{82}$$

The fidelity is then

$$F = \prod_{k \in S_L} \cos(\theta_k(m_+) - \theta_k(m_-)), \tag{83}$$

where $\theta_k(m_\pm)$ is the value θ_k with mass $m_0 \pm \delta/2$. Most of the terms in the product formula for the fidelity are equal to one up to numerical precision for any mass, but near $m_0 = 0$ there are deviations which are most prominent at the longest wavelength, namely $|k| = 1/2$. Approximating the fidelity at criticality by the overlap on this single pair of modes and assuming $1/\delta, V \gg 1$ results in

$$F \approx 1 - \frac{\delta^2 V^2}{8\pi^2}, \qquad m_0 = 0, \tag{84}$$

where the derivative coefficients have been summed as in Eq. (33). By contrast, away from criticality, letting $\delta = 1/V$,

$$F \approx 1 - \frac{\pi^2 \delta^2}{8 m_0^4 V^2}, \qquad |m_0| \gg 1/V, \tag{85}$$

which quickly approaches 1.

Rather than computing the fidelity overlap of the global ground states, an approximation can be obtained in a multiresolution wavelet basis by computing the fidelity overlap between reduced states of a few coarse modes. This reduced state effectively acts as a compressed representation of the global state. Specifically, the fidelity between reduced states is given by

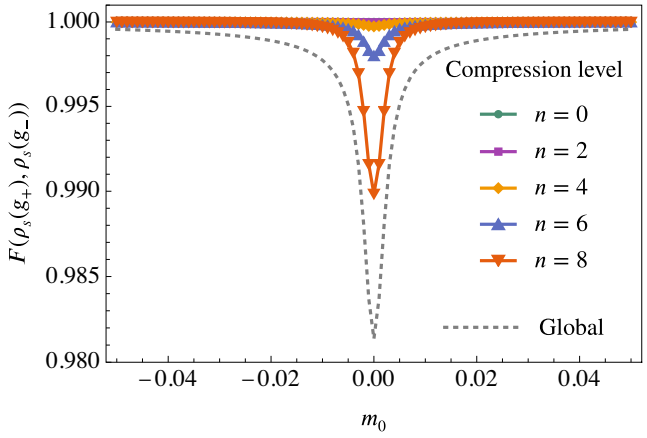

FIG. 6. Fidelity of a 2-mode subsystem of scale modes at scale $r = 0$ in a multiscale representation of the ground state of the fermionic QFT as a function of wavelet transform level n. Here we keep $V = 1024$ and $\delta = 1/V$ constant. Daubechies $\mathcal{K} = 3$ wavelets were used. The dashed grey line is the analytic expression for the fidelity overlap of the global state from Eq. (83). The phase transition at $m_0 = 0$ is increasingly evident for higher compression levels.

$$F(\rho_s(g_+), \rho_s(g_-)) = \mathrm{Tr}\left[\sqrt{\sqrt{\rho_s(g_+)}\rho_s(g_-)\sqrt{\rho_s(g_+)}}\right], \tag{86}$$

where $\rho_s(g)$ is the reduced state on subsystem s of the global pure state $|\Psi(g)\rangle$. For the fermionic Ising model field theory, the fidelity between two mixed fermionic Gaussian states with covariance matrices $\Gamma_s(g_+), \Gamma_s(g_-)$ (expressed as covariances in the Majorana representation) is given by [30]

$$F = \frac{\det[\mathbb{1} + \sqrt{e^{\tanh^{-1}\Gamma_s(g_+)} e^{2\tanh^{-1}\Gamma_s(g_-)} e^{\tanh^{-1}\Gamma_s(g_+)}}]^{1/2}}{\det[\mathbb{1} + e^{2\tanh^{-1}\Gamma_s(g_+)}]^{1/4} \det[\mathbb{1} + e^{2\tanh^{-1}\Gamma_s(g_-)}]^{1/4}}. \tag{87}$$

In Fig. 6 the signature of a QPT is evident in the fidelity overlap calculated between two-mode subsystems of coarse modes. As expected, the minimum occurs at $m_0 = 0$ and is considerably more significant for subsystems of coarser modes (corresponding to higher wavelet transform levels) compared to finer modes.

We note also a dependence on the Daubechies wavelet index $\mathcal{K}$, such that higher wavelet indices provide a better approximation to the whole-state/analytic behavior with only a few coarse modes (i.e., a lower fidelity minimum). However in the case of calculating the fidelity overlap the effect is weak, of order 10^{-5}, and becomes weaker for higher $\mathcal{K}$.

E. Holographic entanglement of purification

Recently there has been progress in connecting entanglement in a boundary quantum field theory to geometric quantities in the bulk dual [10,18,31]. A particularly compelling idea inspired by holographic duality is the conjectured equality [18]

$$E_p(\rho_{AB}) \stackrel{?}{=} E_W(\rho_{AB}), \tag{88}$$

where $E_p(\rho_{AB})$ is the entanglement of purification of a subsystem ρ_{AB} of a boundary CFT, and $E_W(\rho_{AB})$ is the entanglement wedge cross section, a geometric quantity defined in the bulk. The entanglement of purification is defined as

$$E_p(\rho_{AB}) = \min_{|\psi\rangle_{A\bar{A}B\bar{B}}; \mathrm{Tr}_{\bar{A}\bar{B}}[|\psi\rangle\langle\psi|] = \rho_{AB}} S(\rho_{A\bar{A}}), \tag{89}$$

where $\bar{A}, \bar{B}$ are auxiliary systems to A, B and the minimum is taken over all purifications $|\psi\rangle$ of the state ρ_{AB}. The entanglement wedge cross section is

$$E_W(\rho_{AB}) = \frac{|\Sigma^*_{AB}|}{4G_N}, \tag{90}$$

where $|\Sigma^*_{AB}|$ is the area of the minimal cross section of the entanglement wedge in the bulk dual that connects the boundary subsystem A with B. We use units where $4G_N = 1$. In the case of a $(1+1)$D boundary CFT, Σ^*_{AB} is a one-dimensional surface.

An appealing feature of the entanglement wedge cross section is that it is blind to cutoff-dependent features of the entanglement entropy due to cancellation of such terms. The motivation for the conjectured equivalence in Eq. (88) is that—assuming that the global state is pure—the entanglement wedge satisfies several inequalities shared by the entanglement of purification (EoP) including

(1) $I(A:B)/2 \leq E_W(\rho_{AB}) \leq \min(S(\rho_A), S(\rho_B))$
(2) $E_W(\rho_{AB}) \leq E_W(\rho_{A(BC)}) \leq E_W(\rho_{AB}) + E_W(\rho_{BC})$
(3) $E_W(\rho_{(AA')(BB')}) \geq E_W(\rho_{AB}) + E_W(\rho_{A'B'})$

The first statement refers to the mutual information

$$I(A:B) = S(\rho_A) + S(\rho_B) - S(\rho_{AB}). \tag{91}$$

The left-hand side of the second statement follows from the extensiveness of the entanglement of mutual information and the right-hand side is a polygamy inequality. Both these inequalities are shared by EoP. The third inequality is a statement of strong superadditivity [18]. EoP in fact satisfies subadditivity: $E_P(\rho \otimes \sigma) \leq E_P(\rho) + E_P(\sigma)$ with equality only if the optimal purification of the joint state $\rho \otimes \sigma$ is the product of optimal purifications of ρ and σ separately, which is expected in holographic CFTs [18], in which case EoP becomes additive like E_W.

In order to better understand holographic entanglement of purification from a wavelet perspective, consider the case of a ground state $(1+1)$D CFT of overall length l and with periodic boundaries. The entanglement wedge cross section has an analytic formula, whereas the entanglement

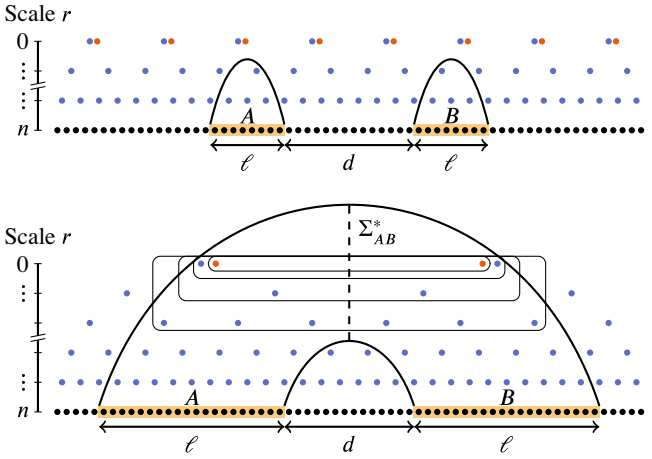

FIG. 7. Illustration of the holographic entanglement features studied in this paper for a ground state of a $(1+1)$D CFT with periodic boundaries. The physical degrees of freedom at the finest scale $r=n$ are represented by scale modes (black). Coarser wavelet modes at scale $r=n-1,\ldots,0$ are shown (blue) as are the coarse scale modes at scale $r=0$ (orange). The representation of the ground state using all the wavelet and coarse scale modes is referred to as the bulk description, and is related by a unitary wavelet transformation to the boundary description using scale modes at scale n. Top: size ℓ of the regions A, B is too small relative to their separation d so that $I(A:B)=0$. There is no entanglement wedge and $E_W(\rho_{AB})=0$. Bottom: here $d/\ell > \sqrt{2}-1$ and there is an entanglement wedge with minimal cross section $|\Sigma^*_{AB}| = E_W(\rho_{AB}) = \frac{c}{6}\log(1+2d/\ell)$. Shown in the smallest ellipse is a bulk subsystem involving only coarse scale modes at scale $r=0$, a larger ellipse involving scale and wavelet modes at scale $r=0$, and so forth. If the subsystems in these smaller sized ellipses accurately capture the mutual information $I(A:B)$ with only a few scales, then we speak of a compressed representation of ρ_{AB}.

of purification does not, rather it involves a complex minimization. To see the former, consider two regions A and B, ordered left to right, separated by a distance d and with equal lengths $|A|=|B|=\ell \ll L$, and with boundary points $\{\partial A_L, \partial A_R, \partial B_L, \partial B_R\}$. The entropy (up to an additive constant) of the joint region $A\cup B$ is given by the minimal length curve in AdS space that separates it from its complement. This will either be the sum of the geodesic connecting boundary points $\{\partial A_L, \partial A_R\}$ and that connecting $\{\partial B_L, \partial B_R\}$ (see Fig. 7, top), i.e., $\frac{2c}{3}\log(\ell)$, or the sum of the geodesic which connects $\{\partial A_L, \partial B_R\}$ and that connecting $\{\partial A_R, \partial B_L\}$ (see Fig. 7, bottom). i.e., $\frac{c}{3}\log(d(d+2\ell))$. These two lengths become degenerate at $d/\ell=\sqrt{2}-1$. The mutual information is then

$$I(A:B)=\begin{cases}0 & d/\ell \geq \sqrt{2}-1\\ -\frac{c}{3}\log((d/\ell)^2+2d/\ell) & d/\ell<\sqrt{2}-1\end{cases}. \tag{92}$$

For regions A, B satisfying $I(A:B)>0$, the entanglement wedge W is the region in the bulk bounded by $A\cup B$ and the minimal length geodesics separating $A\cup B$ from its complement (Fig. 7, bottom). The entanglement wedge cross section $|\Sigma^*_{AB}|$ is the length of the shortest curve Σ_{AB} in AdS space that divides the wedge into two pieces: one containing A, the other B. Because the AdS distance from the midpoint of a geodesic to the boundary point bisecting the boundary curve is one half the length of the geodesic, the entanglement wedge cross section is therefore (for the example above)

$$E_W(\rho_{AB}) = \frac{c}{6}\log(1+2\ell/d). \tag{93}$$

In terms of the bulk modes, we seek to compute the entanglement of purification $E_p(\rho_{AB})$ via a compressed representation of ρ_{AB} only involving a few coarse scale and wavelet modes. As illustrated in Fig. 7 (bottom), if small bulk subsystems accurately capture the mutual information $I(A:B)$ then it will suffice to restrict to this small compressed subsystem to calculate the entanglement of purification. Ideally, if the state ρ_{AB} is represented only in terms of two coarse scale modes and two coarse wavelet modes both at scale $l_{\min}$ then it may be possible to analytically compute $E_P(\rho_{AB})$.

Following the scheme in Fig. 7 (bottom) we study some examples of subsystem sizes ℓ and separations d that have nonzero mutual information calculated using the boundary scale modes at scale n, under the assumption $\ell, d \ll L$. By computing a wavelet transform on the covariance matrix we find cases where $I(A:B)$ is accurately represented by a few coarse scale and wavelet modes, as demonstrated in Fig. 8.

Assume there exists a state for which $I(A:B)$ is well approximated up to some small additive error by a compression to two coarse scale modes (one for A and one for B), and let the reduced two-mode state be

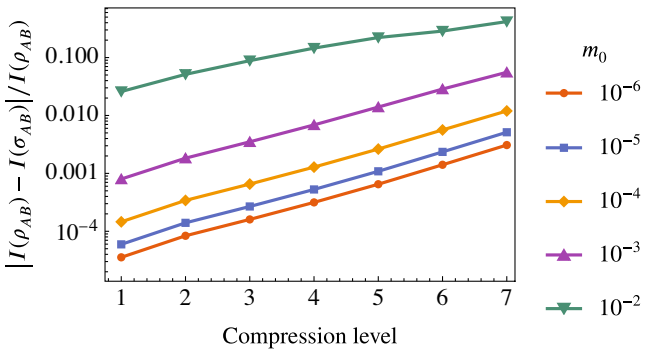

FIG. 8. Relative error of approximating the mutual information $I(A:B)$ by the wavelet compressed representation σ_{AB} of the reduced state ρ_{AB}, where A and B are subsystems of the ground state of a $(1+1)$-dimensional scalar bosonic field theory with a total system size of $V=4096$. The subsystems are chosen to have a separation of inner boundaries by a length $d=512$ and are of equal size $\ell=|A|=|B|=256$. For each additional compression the number of degrees of freedom is halved.

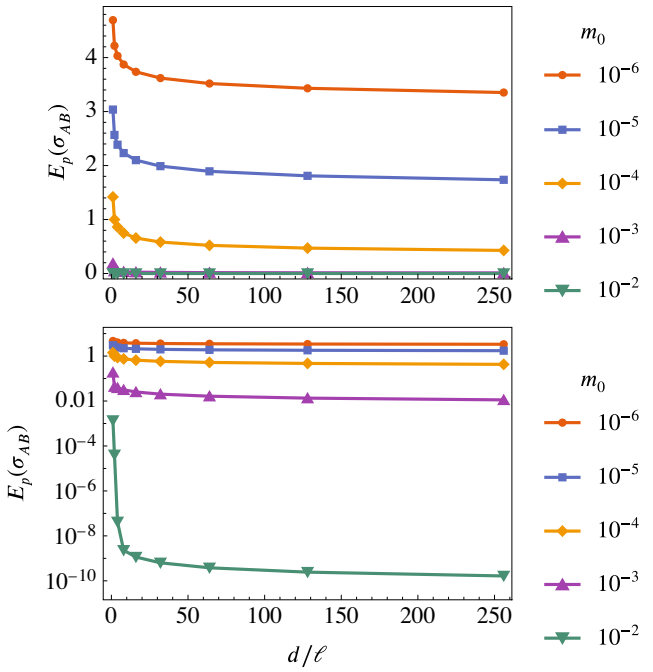

FIG. 9. Top: entanglement of purification $E_p(\sigma_{AB})$ as a function of the ratio d/ℓ as captured by wavelet compression of the ground state as in Fig. 8. Here σ_{AB} is the reduced state represented by two coarse grained scale modes obtained by the wavelet transformation on the covariance matrix representation of ρ_{AB}. The separation between subsystems $d = 512$ is fixed, and $\ell = |A| = |B|$ is varied from 512 to 2. The compressed state allows for a calculation of entanglement of purification in terms of a one parameter minimization. Bottom: same as top but on a log scale. Compare with Bhattacharyya *et al.* [31] (Fig. 6 there).

denoted σ_{AB}. Calculating $E_P(\sigma_{AB})$ following the method of Bhattacharyya *et al.* (Sec. 4.1 in [31]) requires minimizing the entropy $S(\sigma_{A\bar{A}})$ over a single real parameter. The corresponding minimization for a state compressed to two coarse scale modes and two coarse wavelet mode (see Sec. 4.3 in [31]) requires minimizing the entropy $S(\sigma_{A\bar{A}})$ over four real parameters. Both these methods assume the minimizing pure state is also Gaussian. This greatly simplifies the analysis, as we can continue to represent states with covariance matrices. The results, plotted in Fig. 9, appear to validate this assumption. The behavior of $E_P(\sigma_{AB})$ is comparable to Eq. (93), the analytic formula for the entanglement wedge cross section $E_W(\rho_{AB})$.

A phase transition also becomes apparent in the value of the single minimization parameter x during the process of minimizing for the entropy $S(\rho_{A\bar{A}})$. Following the approach in Bhattacharyya *et al.* [31], consider a pure state on a total system $A\bar{A}B\bar{B}$ with covariance matrices

$$\Gamma^{\Pi\Pi}_{AB\bar{A}\bar{B}} = \frac{1}{2}\begin{pmatrix} J & K \\ K^T & L \end{pmatrix}, \quad \Gamma^{\Phi\Phi}_{AB\bar{A}\bar{B}} = \frac{1}{2}\begin{pmatrix} D & E \\ E^T & F \end{pmatrix} \tag{94}$$

such that

$$\begin{pmatrix} J & K \\ K^T & L \end{pmatrix}^{-1} = \begin{pmatrix} D & E \\ E^T & F \end{pmatrix}. \tag{95}$$

The matrices are written in the basis $(\Phi_{AB}, \Phi_{\bar{A}\bar{B}})$, where the known reduced state covariance matrices are $\Gamma^{\Pi\Pi}_{AB} = \frac{1}{2}J$ and $\Gamma^{\Phi\Phi}_{AB} = \frac{1}{2}D$. Now it follows from Eq. (95) that

$$\begin{aligned} JD + KE^T &= K^T E + LF = \mathbb{1}, \\ JE + KF &= K^T D + LE^T = 0, \end{aligned} \tag{96}$$

which implies $L = -K^T D(\mathbb{1} - JD)^{-1}K$. Hence given the covariance matrix Γ_{AB} the purified state covariance matrix is completely specified by K. The dimensions of K will depend on the size of the auxiliary spaces $\bar{A}\,\bar{B}$. Bhattacharyya *et al.* [31] show that for the case where $|A| = |B| = 1$, an accurate value of the entanglement of purification can be obtained by choosing $|\bar{A}| = |\bar{B}| = 1$, meaning that the value obtained is negligibly changed by choosing larger auxiliary systems. Furthermore, by invoking exchange symmetry of A and B, K can be chosen to have the canonical form

$$K = \begin{pmatrix} 1 & x \\ x & 1 \end{pmatrix} \tag{97}$$

where $x \in (-1, 1)$. The value of x should be selected in order to minimize the entropy of the reduced state of $A\bar{A}$ described from the reduced covariance matrix $\Gamma_{A\bar{A}}$ which is found by tracing out rows and columns of $\Gamma_{AB\bar{A}\bar{B}}$.

A plot of the value of the parameter x that minimizes the entropy of the reduced state $A\bar{A}$ is shown in Fig. 10 for several decades of mass. There is a notable peak in the value of x at the subregion size to separation distance ratio $d/\ell = 2$, indicative of a phase transition near that value.

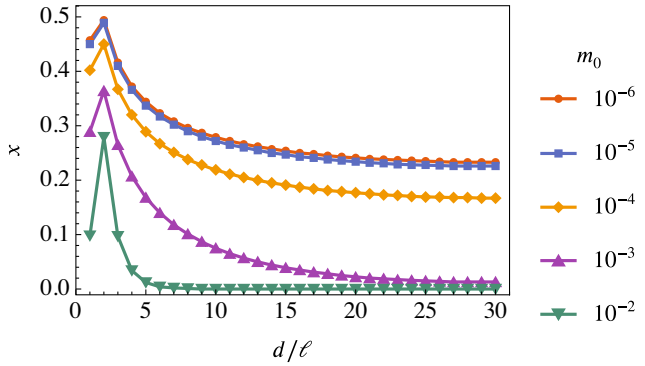

FIG. 10. Minimizing value x for the entanglement of purification of a compressed ground state as in Fig. 9 plotted as a function of d/ℓ, focusing on the region $d/\ell \leq 30$. The peak in the value at $d/\ell = 2$ is indicative of a phase transition near that ratio.

V. DISCUSSION

We show in result IV A that the same-scale correlators in the multiscale representation of the ground states for the bosonic and fermionic theories demonstrate the expected power-law decay in the massless case, with an exponent that depends on the Daubechies index $\mathcal{K}$, and exponential decay in the massive cases. Mass renormalization is naturally emergent as a function of scale. We also consider in result IV B the entanglement features of the ground states of the two QFTs in a scale field representation and verified that the Calabrese-Cardy relations are obeyed. For the massive bosonic theory in 1D and 2D, we observe that the entanglement entropy of a subsystem is constant as a function of the subsystem's length in different scales. The constant value increases as we increase the scale parameter k as is to be expected from the entanglement area law. For the massless bosonic and fermionic CFTs, we obtain the correct central charges and also the cutoff dependence of the entropy as a function of scale.

Results IV D and IV E demonstrate two potential applications of using a wavelet-based multiscale representation as a form of compression, where some function on a system with $2^n X$ modes can be approximated by applying that function to a reduced state of X coarse scale modes obtained from an n-level wavelet transform.

In the case of result IV D, we show that in a fermionic QFT this wavelet compression technique can be used to identify a phase transition, evident in a decrease in fidelity overlap between ground states adjacent in some parameter space (here, mass). Given that the fast wavelet transform (FWT) has an efficient classical implementation that scales with $\mathcal{O}(N\log(N))$, where N is the dimension of the vector space, this technique holds promise for approximating the value of a many-body observable that might otherwise be prohibitively difficult to observe directly due to experimental, computational, or other constraints.

Finally, result IV E demonstrates that, for a bosonic QFT, wavelet compression qualitatively captures the physics of the mutual information between isolated subsystems, including identification of a phase transition.

The use of higher-order wavelet basis functions results in more desirable mathematical properties, such as increased accuracy of approximations using a small number of modes, and well-defined higher-order derivatives, at the cost of moderately increased computational complexity. As noted in Beylkin and Keiser [32] (page 179), the error incurred by the wavelet discretization method on a second-order differential equation described by a Laplacian is $\mathcal{O}((\Delta x)^{2\mathcal{K}})$ where $\Delta x = 2^{-k}$ and k is the number of scales in the multiresolution analysis. We can extrapolate this point to the bosonic field theory for an $\mathcal{O}(2^{-2k\mathcal{K}})$ error scaling, and to the fermionic field theory (arises from a first-order equation) to find an error scaling of $\mathcal{O}(2^{-k\mathcal{K}})$. This suggests that we have a strategy for reducing error in the discretization that is not simply increasing the number of scales k, i.e., reducing the size of the length cutoff. We may also reduce error by increasing the value of $\mathcal{K}$. Note however that increasing $\mathcal{K}$ results in a corresponding computational cost since the number of nonzero bands in the associated wavelet transform scales as $2\mathcal{K}$.

In this paper we have mostly used a uniform wavelet basis with either periodic or antiperiodic boundary conditions. This conforms to the usual application of the discrete wavelet transform with periodic/antiperiodic signal extension modes in numerical signal processing. In the case of Sec. IV B, the application of open boundaries corresponds to the absence of a signal extension, which is sufficient for the calculation of bulk entanglement since this property is sensitive primarily to the underlying topology of the space. However, when studying open or nonperiodic systems with essential physics at the boundaries, for example, symmetry-protected topological phases [33], then a careful consideration of the wavelet representation of that theory at the boundaries is necessary. For an overview of boundary wavelet construction, see Mallat [21] (pages 322–328).

VI. CONCLUSION

We have demonstrated the utility of wavelet analysis when describing quantities such as entanglement in fermionic and bosonic QFTs. Specifically, the scale dependence of various quantities such as subsystem entropy and correlations emerge simply by fixing a wavelet basis, unlike, for example, tensor network representations, where generally the elements of the tensors must be obtained by numerical optimization. We have additionally shown that wavelets provide a way to compress quantum states in a way that enables the calculation of quantum informational quantities on a very few number of modes. Such a result could be useful in experimental probes of quantum simulations of QFTs where measuring observables over an extensive number of modes is costly or error prone.

Wavelet analyses have potential in more general QFT simulation algorithms, and are already showing promise in algorithms for ground state generation with spatial inhomogeneities [23]. By showing that cutoff-dependent results like those of Calabrese and Cardy [1] appear directly as a function of an input scale parameter in wavelet-based representations of QFT, we bolster the case for wavelet-based representations as a key tool of analysis for the physics of quantum fields.

ACKNOWLEDGMENTS

Y. R. S. thanks Eric Howard for many helpful discussions on lattice regularization and entanglement area laws. G. K. B. acknowledges helpful discussions with Dean Southwood. D. J. G. and G. K. B. acknowledge support

from the Australian Research Council (ARC) through Grant No. DP200102152 and from the ARC Centre of Excellence for Engineered Quantum Systems (EQUS, CE170100009). D. J. G. was supported by the Sydney Quantum Academy, Sydney, Australia. M. B. and B. C. S. acknowledge support from the Government of Alberta and by the Natural Sciences and Engineering Research Council of Canada (NSERC).

APPENDIX: EXPRESSIONS FOR FERMIONIC CONVARIANCE MATRIX

1. General solution in wavelet scale basis

The Hamiltonian for the Ising model field theory in the continuous case is

$$\hat{H} = \frac{1}{2}\int dx[\hat{\boldsymbol{c}}^\dagger(x)\mathrm{i}Y\partial_x\hat{\boldsymbol{c}}(x) + m_0\hat{\boldsymbol{c}}^\dagger(x)Z\hat{\boldsymbol{c}}(x)], \tag{A1}$$

where $\mathrm{i}Y = \left(\begin{smallmatrix}0 & 1\\ -1 & 0\end{smallmatrix}\right)$, $Z = \left(\begin{smallmatrix}1 & 0\\ 0 & -1\end{smallmatrix}\right)$ and the fermionic field operators are $\hat{\boldsymbol{c}}(x) = \left(\begin{smallmatrix}\hat{c}(x)\\ \hat{c}^\dagger(x)\end{smallmatrix}\right)$, $\hat{\boldsymbol{c}}^\dagger(x) = (\hat{c}^\dagger(x)\ \hat{c}(x))$, with the anticommutation relation $\{\hat{c}(x), \hat{c}^\dagger(x')\} = \delta(x-x')$. Discretising the continuous Hamiltonian into $2^n X = V$ scale modes $\hat{\boldsymbol{r}}_\ell = \left(\begin{smallmatrix}\hat{r}_\ell\\ \hat{r}_\ell^\dagger\end{smallmatrix}\right)$ where $\hat{r}_\ell = \hat{r}_\ell^{(n;s)} = \int dx s_\ell^{(n)}(x)\hat{c}(x)$ and $\{\hat{r}_\ell, \hat{r}_{\ell'}^\dagger\} = \delta_{\ell,\ell'}$ gives the discrete Hamiltonian in the scale-n basis

$$\hat{H}^{(n)} = \frac{1}{2}\sum_{\ell=0}^{V-1}\left[\sum_{j=-2\mathcal{K}+2}^{2\mathcal{K}-2}\hat{\boldsymbol{r}}_\ell^\dagger \mathrm{i}Y\Delta_j^{(1)}\hat{\boldsymbol{r}}_{\ell+j} + m_0\hat{\boldsymbol{r}}_\ell^\dagger Z\hat{\boldsymbol{r}}_\ell\right], \tag{A2}$$

where $\mathcal{K}$ is the Daubechies wavelet index and $\Delta_j^{(1)} \equiv \Delta_{\ell,\ell+j}^{(1)}$ is the first derivative operator in the base scale [scale-0 as per Eq. (12)] and is nonzero only when $-2\mathcal{K}+2 \le j \le 2\mathcal{K}-2$.

Note that $\hat{H}$ commutes with the total fermionic parity operator $\hat{J} = \prod_\ell (1 - 2\hat{r}_\ell^\dagger\hat{r}_\ell)$, and in order to have translational invariance on the even parity sector, application of antiperiodic boundary conditions requires $\hat{r}_{V+\ell} \equiv -\hat{r}_\ell$. In practice this means that the upper-right and lower-left corner terms in the matrix $\Delta^{(1)}$ will be the negative of those along the corresponding main diagonals.

This Hamiltonian can be expressed in terms of uncoupled modes $\hat{\eta}_k$ in the usual diagonal form as follows:

$$\hat{H} = \sum_{k\in S}\omega_k\left(\hat{\eta}_k^\dagger\hat{\eta}_k - \frac{1}{2}\right) \tag{A3}$$

where $S = \{\frac{1}{2}, \frac{3}{2}, \ldots, V-\frac{1}{2}\}$ due to the antiperiodic boundary conditions. The ground state $|G\rangle$ is defined by $\hat{\eta}_k|G\rangle = 0$, from which follow the uncoupled correlations $\langle\hat{\eta}_k\hat{\eta}_{k'}\rangle = \langle\hat{\eta}_k^\dagger\hat{\eta}_{k'}^\dagger\rangle = \langle\hat{\eta}_k^\dagger\hat{\eta}_{k'}\rangle = 0$, and $\langle\hat{\eta}_k\hat{\eta}_{k'}^\dagger\rangle = \delta_{k,k'}$.

The uncoupled modes $\hat{\eta}_k$ are related to the original fermionic modes $\hat{r}_\ell$ via a pair of transforms. The original modes are related to the momenta modes by the usual Fourier transform $\hat{p}_k = \frac{1}{\sqrt{V}}\sum_{\ell=0}^{V-1}\hat{r}_\ell \mathrm{e}^{\mathrm{i}2\pi k\ell/V}$. The momenta modes are related to the uncoupled modes by way of the Bogoliubov transform $\hat{\eta}_k = u_k\hat{p}_k + \mathrm{i}v_k\hat{p}_{-k}^\dagger$, where $u_k = -(m_0+\omega_k)/\sqrt{(m_0+\omega_k)^2+q_k^2}$, $v_k = q_k/\sqrt{(m_0+\omega_k)^2+q_k^2}$, $\omega_k = \sqrt{m_0^2+q_k^2}$ (ω_k are the eigenvalues of the Hamiltonian) and $q_k = 2\sum_{j=1}^{2\mathcal{K}-2}\Delta_j^{(1)}\sin\frac{2\pi jk}{V}$. The combined transform can be expressed in the form:

$$\hat{\eta}_k = \frac{u_k}{\sqrt{V}}\sum_{\ell=0}^{V-1}\hat{r}_\ell \mathrm{e}^{\mathrm{i}2\pi k\ell/V} + \frac{\mathrm{i}v_k}{\sqrt{V}}\sum_{\ell=0}^{V-1}\hat{r}_\ell^\dagger \mathrm{e}^{\mathrm{i}2\pi k\ell/V}. \tag{A4}$$

Introduce the Majorana scale modes $\hat{\boldsymbol{b}}_\ell = \left(\begin{smallmatrix}\hat{b}_{\ell,0}\\ \hat{b}_{\ell,1}\end{smallmatrix}\right)$ with $\hat{b}_{\ell,0} = \hat{b}_{\ell,0}^{(n;s)} = \hat{r}_\ell + \hat{r}_\ell^\dagger$, $\hat{b}_{\ell,1} = \hat{b}_{\ell,1}^{(n;s)} = -\mathrm{i}(\hat{r}_\ell - \hat{r}_\ell^\dagger)$, such that $\{\hat{b}_{\ell,\sigma}, \hat{b}_{\ell',\sigma'}\} = 2\delta_{\ell,\ell'}\delta_{\sigma,\sigma'}$. The Hamiltonian transforms to

$$\hat{H}^{(n)} = -\frac{1}{4}\sum_{\ell=0}^{V-1}\left[\sum_{j=-2\mathcal{K}+2}^{2\mathcal{K}-2}\hat{\boldsymbol{b}}_\ell^T\mathrm{i}X\Delta_j^{(1)}\hat{\boldsymbol{b}}_{\ell+j} + m_0\hat{\boldsymbol{b}}_\ell^T Y\hat{\boldsymbol{b}}_\ell\right]. \tag{A5}$$

That $u_k = u_{-k}$ and $v_k = -v_{-k}$ follows from the properties of the Bogoliubov transform. Furthermore introduce θ_k such that $u_k = \cos\theta_k$, $v_k = \sin\theta_k$, and so

$$\begin{aligned}\hat{\eta}_k + \hat{\eta}_{-k}^\dagger &= \frac{\mathrm{e}^{\mathrm{i}\theta_k}}{\sqrt{V}}\sum_{\ell=0}^{V-1}\hat{b}_{\ell,0}\mathrm{e}^{\mathrm{i}2\pi k\ell/V},\\ \hat{\eta}_k - \hat{\eta}_{-k}^\dagger &= \frac{\mathrm{i}\mathrm{e}^{-\mathrm{i}\theta_k}}{\sqrt{V}}\sum_{\ell=0}^{V-1}\hat{b}_{\ell,1}\mathrm{e}^{\mathrm{i}2\pi k\ell/V},\end{aligned} \tag{A6}$$

$$\begin{aligned}\hat{b}_{\ell,0} &= \frac{1}{\sqrt{V}}\sum_{k\in S}\mathrm{e}^{-\mathrm{i}\theta_k}(\hat{\eta}_k + \hat{\eta}_{-k}^\dagger)\mathrm{e}^{-\mathrm{i}2\pi k\ell/V},\\ \hat{b}_{\ell,1} &= \frac{1}{\sqrt{V}}\sum_{k\in S} -\mathrm{i}\mathrm{e}^{-\mathrm{i}\theta_k}(\hat{\eta}_k - \hat{\eta}_{-k}^\dagger)\mathrm{e}^{-\mathrm{i}2\pi k\ell/V}.\end{aligned} \tag{A7}$$

Noting that $\theta_{-k} = \arctan(v_{-k}/u_{-k}) = \arctan(-v_k/u_k) = -\theta_k$, the correlations can now be computed directly:

$$\begin{aligned}\langle\hat{b}_{\ell,0}\hat{b}_{\ell',0}\rangle &= \frac{1}{V}\sum_{k,k'\in S}\mathrm{e}^{-\mathrm{i}(\theta_k+\theta_{k'})}\mathrm{e}^{-\mathrm{i}2\pi(k\ell+k'\ell')/V}\\ &\quad\times\underbrace{\langle(\hat{\eta}_k + \hat{\eta}_{-k}^\dagger)(\hat{\eta}_{k'} + \hat{\eta}_{-k'}^\dagger)\rangle}_{=\delta_{k,-k'}}\\ &= \delta_{\ell,\ell'}\end{aligned} \tag{A8}$$

$$\langle \hat{b}_{\ell,0}\hat{b}_{\ell',1}\rangle = \frac{\mathrm{i}}{V}\sum_{k,k'\in S} \mathrm{e}^{-\mathrm{i}(\theta_k-\theta_{k'})}\mathrm{e}^{-\mathrm{i}2\pi(k\ell+k'\ell')/V} \times \underbrace{\langle(\hat{\eta}_k+\hat{\eta}^\dagger_{-k})(\hat{\eta}_{k'}-\hat{\eta}^\dagger_{-k'})\rangle}_{=-\delta_{k,-k'}} = \frac{\mathrm{i}}{V}\sum_{k\in S}\mathrm{e}^{-2\mathrm{i}\theta_k}\mathrm{e}^{-\mathrm{i}2\pi(\ell-\ell')k/V}. \tag{A9}$$

Similarly $\langle \hat{b}_{\ell,1}\hat{b}_{\ell',1}\rangle = \delta_{\ell,\ell'}$ and $\langle \hat{b}_{\ell,1}\hat{b}_{\ell',0}\rangle = -\langle \hat{b}_{\ell,0}\hat{b}_{\ell',1}\rangle$. The covariance matrix Γ defined as $\langle \hat{b}_{\ell,\sigma}\hat{b}_{\ell',\sigma'}\rangle = \delta_{\ell,\ell'}\delta_{\sigma,\sigma'} + \mathrm{i}\Gamma_{\sigma,\ell;\sigma'\ell'}$ in the basis $|\sigma\rangle|\ell\rangle, \sigma\in\{0,1\}$ is therefore

$$\Gamma_{\sigma,\ell;\sigma',\ell'} = \begin{bmatrix} 0 & \Gamma^{01} \\ -(\Gamma^{01})^T & 0 \end{bmatrix}, \tag{A10}$$

$$\Gamma^{01}_{\ell,\ell'} = \frac{1}{V}\sum_{k\in S}\mathrm{e}^{-2\mathrm{i}\theta_k}\mathrm{e}^{-\mathrm{i}2\pi(\ell-\ell')k/V}, \tag{A11}$$

with $\theta_k = \arctan\frac{-q_k}{m_0+\sqrt{m_0^2+q_k^2}}$ and $q_k = 2\sum_{j=1}^{2\mathcal{K}-2}\Delta_j^{(1)}\sin\frac{2\pi jk}{V}$.

2. Zero-mass limit

Consider the zero-mass limit $m_0 \to 0$:

$$\lim_{m_0\to 0}\theta_k = \lim_{m_0\to 0}\arctan\frac{-q_k}{m_0+\sqrt{m_0^2+q_k^2}} = -\frac{\pi}{4}\mathrm{sgn}q_k = \begin{cases}\frac{\pi}{4} & k\in S_L \\ -\frac{\pi}{4} & k\in S_U\end{cases} \tag{A12}$$

where S_L is the lower half of momenta modes $S_L:\{\frac{1}{2},\frac{3}{2},\ldots,\frac{V-1}{2}\}$ and S_U is the upper half $S_U:\{\frac{V+1}{2},\frac{V+3}{2},\ldots,\frac{2V-1}{2}\}$. The covariance matrix is then

$$\lim_{m_0\to 0}\Gamma^{01}_{\ell,\ell'} = -\frac{\mathrm{i}}{V}\left[\sum_{k\in S_L}\mathrm{e}^{-\mathrm{i}2\pi(\ell-\ell')k/V} - \sum_{k\in S_U}\mathrm{e}^{-\mathrm{i}2\pi(\ell-\ell')k/V}\right]. \tag{A13}$$

Let $\zeta = \mathrm{e}^{-\mathrm{i}\pi(\ell-\ell')/V}$, then

$$\lim_{m_0\to 0}\Gamma^{01}_{\ell,\ell'} = -\frac{\mathrm{i}}{V}[(\zeta+\zeta^3+\cdots+\zeta^{V-1}) - (\zeta^{V+1}+\zeta^{V+3}+\cdots+\zeta^{2V-1})], \tag{A14}$$

$$\lim_{m_0\to 0}(\zeta^2\Gamma^{01}_{\ell,\ell'} - \Gamma^{01}_{\ell,\ell'}) = -\frac{\mathrm{i}}{V}[-\zeta+\zeta^{V+1}+\zeta^{V+1}-\zeta^{2V+1}], \tag{A15}$$

$$\lim_{m_0\to 0}\Gamma^{01}_{\ell,\ell'} = -\frac{\mathrm{i}}{V}\frac{1}{\zeta-\zeta^{-1}}(2\mathrm{e}^{-\mathrm{i}\pi(\ell-\ell')}-2) \tag{A16}$$

$$= \begin{cases}\frac{-2}{V\sin(\pi(\ell-\ell')/V)} & \ell-\ell' \text{ odd} \\ 0 & \ell-\ell' \text{ even}\end{cases}. \tag{A17}$$

3. Finite mass

For finite mass, define $s_k = q_k/m_0$. Then for $m_0 \gg |q_k|$, $\theta_k = \arctan\left(-s_k/\left(1+\sqrt{1+s_k^2}\right)\right) \approx -s_k/2 + O(s_k^3)$, and so

$$\Gamma^{01}_{\ell,\ell'} = \frac{1}{V}\sum_{k\in S}\mathrm{e}^{\mathrm{i}s_k}\mathrm{e}^{-\mathrm{i}2\pi(\ell-\ell')k/V}. \tag{A18}$$

In the special case of Haar wavelets ($\mathcal{K}=1$), $\Delta_1^{(1)} = -\frac{1}{2}$, $\Delta^{(1)}_{\ell>1} = 0$, and so $s_k = -\frac{1}{m_0}\sin(2\pi k/V)$:

$$\Gamma^{01}_{\ell,\ell'} = \frac{1}{V}\sum_{k\in S}\mathrm{e}^{-\frac{\mathrm{i}}{m_0}\sin(2\pi k/V)}\mathrm{e}^{-\mathrm{i}2\pi(\ell-\ell')k/V}, \tag{A19}$$

$$\lim_{V\to\infty}\Gamma^{01}_{\ell,\ell'} = \frac{1}{2\pi}\int_0^{2\pi}\mathrm{e}^{\mathrm{i}(-\frac{1}{m_0}\sin k-(\ell-\ell')k)}dk \tag{A20}$$

$$= J_{\ell-\ell'}\left(-\frac{1}{m_0}\right), \tag{A21}$$

where J is the Bessel function of the first kind. Note also that $J_{-\alpha}(\frac{1}{m_0}) = (-1)^\alpha J_\alpha(\frac{1}{m_0})$.

For $\frac{1}{m_0} \ll \sqrt{|\ell-\ell'|+1}$,

$$J_\alpha\left(\frac{1}{m_0}\right) \approx \frac{1}{\Gamma(\alpha+1)}\left(\frac{1}{2m_0}\right)^\alpha = \frac{1}{\alpha!}\left(\frac{1}{2m_0}\right)^\alpha \approx \frac{1}{\sqrt{2\pi\alpha}}\mathrm{e}^{\alpha(1-\ln 2m_0\alpha)} \tag{A22}$$

And so,

$$\lim_{V\to\infty}\Gamma^{01}_{\ell,\ell'} \approx \frac{1}{\sqrt{2\pi(\ell-\ell')}}\mathrm{e}^{(\ell-\ell')(1-\ln 2m_0(\ell-\ell'))}. \tag{A23}$$

Alternatively, in the limit as the number of modes $V\to\infty$, Eq. (A11) becomes

$$\lim_{V\to\infty}\Gamma^{01}_{\ell,\ell'} = \frac{1}{2\pi}\int_0^{2\pi} e^{-i(2\theta_k+(\ell-\ell')k)}dk \tag{A24}$$

$$= \frac{1}{2\pi}\left(\int_0^{\pi} e^{-i(2\theta_k+(\ell-\ell')k)}dk + \int_0^{\pi} e^{i(2\theta_k+(\ell-\ell')k)}dk\right) \tag{A25}$$

$$= \frac{1}{\pi}\int_0^{\pi}\cos\left(2\theta_k+(\ell-\ell')k\right)dk, \tag{A26}$$

where, as before, $\theta_k = \arctan\left(-q_k/\left(m_0+\sqrt{m_0^2+q_k^2}\right)\right)$ and q_k has been redefined to $q_k = 2\sum_{j=1}^{2\mathcal{K}-2}\Delta_j^{(1)}\sin(jk)$. Letting $\theta_k = \arctan(A_k)$, $A_k = -q_k/\left(m_0+\sqrt{m_0^2+q_k^2}\right)$, this can be further simplified to

$$\lim_{V\to\infty}\Gamma^{01}_{\ell,\ell'} = -\frac{2}{\pi}\int_0^{\pi}\frac{A_k}{1+A_k^2}(A_k\cos((\ell-\ell')k) + \sin((\ell-\ell')k))dk \tag{A27}$$

$$= \begin{cases} -\frac{4}{\pi}\int_0^{\pi/2} B_k\sin((\ell-\ell')k)dk, & \ell-\ell' \text{ odd} \\ -\frac{4}{\pi}\int_0^{\pi/2} C_k\cos((\ell-\ell')k)dk, & \ell-\ell' \text{ even} \end{cases},$$

$$B_k = \frac{A_k}{1+A_k^2}, \qquad C_k = \frac{A_k^2}{1+A_k^2}. \tag{A28}$$

In the special case of Haar wavelets ($\mathcal{K}=1$), $\Delta_1^{(1)} = -\frac{1}{2}$, $\Delta_{\ell>1}^{(1)} = 0$, and so $q_k = -\sin(2\pi k/V)$. The above then simplifies to

$$B_k = \frac{\sin k(m_0+\sqrt{m_0^2+\sin^2 k})}{\sin^2 k+(m_0+\sqrt{m_0^2+\sin^2 k})^2}, \tag{A29}$$

$$C_k = \frac{\sin^2 k}{\sin^2 k+(m_0+\sqrt{m_0^2+\sin^2 k})^2}. \tag{A30}$$

[1] P. Calabrese and J. Cardy, Entanglement entropy and quantum field theory, J. Stat. Mech. (2004) P06002.
[2] S. P. Jordan, K. S. M. Lee, and J. Preskill, Quantum algorithms for quantum field theories, Science **336**, 1130 (2012).
[3] G. Vidal, Class of Quantum Many-Body States that Can Be Efficiently Simulated, Phys. Rev. Lett. **101**, 110501 (2008).
[4] B. Reznik, Entanglement from the vacuum, Found. Phys. **33**, 167 (2003).
[5] L. J. Henderson and N. C. Menicucci, Bandlimited entanglement harvesting, Phys. Rev. D **102**, 125026 (2020).
[6] F. Bulut and W. N. Polyzou, Wavelets in field theory, Phys. Rev. D **87**, 116011 (2013).
[7] G. K. Brennen, P. Rohde, B. C. Sanders, and S. Singh, Multiscale quantum simulation of quantum field theory using wavelets, Phys. Rev. A **92**, 032315 (2015).
[8] X.-L. Qi, Exact holographic mapping and emergent spacetime geometry, arXiv:1309.6282.
[9] C. H. Lee and X.-L. Qi, Exact holographic mapping in free fermion systems, Phys. Rev. B **93**, 035112 (2016).
[10] C. H. Lee, Generalized exact holographic mapping with wavelets, Phys. Rev. B **96**, 245103 (2017).
[11] S. Singh and G. K. Brennen, Holographic construction of quantum field theory using wavelets, arXiv:1606.05068.
[12] G. Evenbly and S. R. White, Entanglement Renormalization and Wavelets, Phys. Rev. Lett. **116**, 140403 (2016).
[13] M. V. Altaisky, Wavelets and renormalization group in quantum field theory problems, Phys. At. Nucl. **81**, 786 (2018).
[14] J. Haegeman, B. Swingle, M. Walter, J. Cotler, G. Evenbly, and V. B. Scholz, Rigorous Free Fermion Entanglement Renormalization from Wavelet Theory, Phys. Rev. X **8**, 011003 (2018).
[15] F. Witteveen and M. Walter, Bosonic entanglement renormalization circuits from wavelet theory, SciPost Phys. **10**, 143 (2021). 2004.11952.
[16] F. Witteveen, V. Scholz, B. Swingle, and M. Walter, Quantum circuit approximations and entanglement renormalization for the Dirac field in $1+1$ dimensions, Commun. Math. Phys. **389**, 75 (2022).
[17] D. Boyanovsky, Field theory of the two-dimensional ising model: Conformal invariance, order and disorder, and bosonization, Phys. Rev. B **39**, 6744 (1989).
[18] K. Umemoto and T. Takayanagi, Entanglement of purification through holographic duality, Nat. Phys. **14**, 573 (2018).
[19] C. Holzhey, F. Larsen, and F. Wilczek, Geometric and renormalized entropy in conformal field theory, Nucl. Phys. **B424**, 443 (1994).
[20] G. Beylkin, On the representation of operators in bases of compactly supported wavelets, SIAM J. Numer. Anal. **29**, 1716 (1992).
[21] S. Mallat, *A Wavelet Tour of Signal Processing* (Elsevier, New York, 2009), 10.1016/B978-0-12-374370-1.X0001-8.
[22] I. Daubechies, *Ten Lectures on Wavelets* (Society for Industrial and Applied Mathematics, Philadelphia, 1992), 10.1137/1.9781611970104.
[23] M. Bagherimehrab, Y. R. Sanders, D. W. Berry, G. K. Brennen, and B. C. Sanders, Nearly optimal quantum algorithm for generating the ground state of a free quantum field theory, PRX Quantum **3**, 020364 (2022).
[24] J. Eisert, M. Cramer, and M. B. Plenio, Colloquium: Area laws for the entanglement entropy, Rev. Mod. Phys. **82**, 277 (2010).

[25] A. Ferraro, S. Olivares, and M. Paris, *Gaussian States in Quantum Information*, Napoli Series on Physics and Astrophysics (Bibliopolis, Napoli, 2005), https://bibliopolis.it/shop/gaussian-states-in-quantum-information/.

[26] K. Meichanetzidis, J. Eisert, M. Cirio, V. Lahtinen, and J. K. Pachos, Diagnosing Topological Edge States via Entanglement Monogamy, Phys. Rev. Lett. **116**, 130501 (2016).

[27] T. F. Demarie, Pedagogical introduction to the entropy of entanglement for gaussian states, Eur. J. Phys. **39**, 035302 (2018).

[28] M. P. Hertzberg, Entanglement entropy in scalar field theory, J. Phys. A **46**, 015402 (2013).

[29] P. Zanardi and N. Paunković, Ground state overlap and quantum phase transitions, Phys. Rev. E **74**, 031123 (2006).

[30] L. Banchi, P. Giorda, and P. Zanardi, Quantum information-geometry of dissipative quantum phase transitions, Phys. Rev. E **89**, 022102 (2014).

[31] A. Bhattacharyya, T. Takayanagi, and K. Umemoto, Entanglement of purification in free scalar field theories, J. High Energy Phys. 04 (2018) 132.

[32] G. Beylkin and J. M. Keiser, An adaptive pseudo-wavelet approach for solving nonlinear partial differential equations, in *Wavelet Analysis and Its Applications* (Elsevier, New York, 1997), Vol. 6, pp. 137–197, 10.1016/S1874-608X(97)80006-4.

[33] X. Chen, Z.-C. Gu, Z.-X. Liu, and X.-G. Wen, Symmetry protected topological orders and the group cohomology of their symmetry group, Phys. Rev. B **87**, 155114 (2013).